

A&A manuscript no.
 (will be inserted by hand later)

Your thesaurus codes are:
20 (11.01.2; 11.03.2; 11.02.1; 11.17.3; 13.18.1; 13.18.2)

**ASTRONOMY
 AND
 ASTROPHYSICS**
 November 18, 2018

Survey of Instantaneous 1–22 GHz Spectra of 550 Compact Extragalactic Objects with Declinations from -30° to $+43^\circ$ *

Y.Y. Kovalev¹, N.A. Nizhelsky², Yu.A. Kovalev¹, A.B. Berlin³, G.V. Zhekanis², M.G. Mingaliev², and A.V. Bogdantsov²

¹ Astro Space Center of the Lebedev Physical Institute, Profsoyuznaya 84/32, Moscow, 119997 Russia

² Special Astrophysical Observatory, Nizhny Arkhyz, Karachaevo-Cherkessia, 357147 Russia

³ Special Astrophysical Observatory, St. Petersburg Branch, St. Petersburg, 196140 Russia

Received March 26; accepted August 13, 1999

Abstract. We present observational results for extragalactic radio sources with milliarcsecond components, obtained with the 600 meter ring radio telescope RATAN–600 from 1st to 22nd December, 1997. For each source, a six frequency broad band radio spectrum was obtained by observing simultaneously with an accuracy up to a minute at 1.4, 2.7, 3.9, 7.7, 13 and 31 cm. The observed list is selected from Preston et al. (1985) VLBI survey and contains all the sources in the declinations between -30° and $+43^\circ$ with a correlated flux density exceeding 0.1 Jy at 13 cm. The sample includes the majority of sources to be studied in the current VSOP survey and the future RadioAstron Space VLBI mission.

Key words: galaxies: active – galaxies: compact – BL Lacertae objects: general – quasars: general – radio continuum: galaxies – radio continuum: general

1. Introduction

One of the main characteristics of an extragalactic radio source is the shape of the broad band spectrum, which provides a considerable amount of physical information about the object. The extragalactic radio sources are often separated into different samples on the basis of the shape of the spectra (e.g. flat, inverted, steep, gigahertz peaked spectrum sources). This shows the importance of the multifrequency broad band spectra surveys of compact extragalactic objects among long term flux variability monitoring programs (e.g. Aller et al. 1985, Mitchell et al. 1994, Stevens et al. 1994, etc.) and VLBI imaging surveys (e.g. Kellermann et al. 1998 and references therein).

Most of the earlier multifrequency spectra results were obtained by combining measurements carried out quasi-

simultaneously (over a period of one or more months) at radio and shorter wavelengths, using several telescopes on some samples of tens of objects, selected by various criteria. For example, we refer to the measurements of 19 active extragalactic sources from 20 cm to 1400 Å by Landau et al. (1986). Valtaoja et al. (1988) investigated quiescent spectra for a sample of 27 radio sources observed at centimeter and millimeter wavelengths. Gear et al. (1994) compared quasi-simultaneous 5–375 GHz spectra of 22 BL Lacertae objects with 24 radio-loud, violently variable quasars. Kühr et al. (1981) compiled radio measurements at more than two frequencies for 494 sources from the combined NRAO–MPI 5 GHz Strong Source Surveys and the Parkes 2.7 GHz Surveys. Herbig & Readhead (1992) composed non-simultaneous radio data from 10 MHz to 100 GHz on a complete sample of 256 objects. We also refer to papers, cited in the O’Dea (1998) survey of compact steep-spectrum and gigahertz peaked-spectrum sources, as well as a number of other works.

Some earlier RATAN–600 results on broad band spectra observations were presented for samples from 8.7 GHz Zelenchuk sky survey by Amirkhanyan et al. (1992) and 87GB survey by Mingaliev & Khabrakhmanov (1995), for strong compact extragalactic objects by Kovalev et al. (1996) and weak radio sources from the RATAN–600 “Cold” deep sky survey by Bursov (1997).

A broad band spectrum of a compact extragalactic radio source is usually considered to be the sum of spectra of several compact and extended components in a source structure. The components are located at various distances from the central nucleus of the object, and are likely to have resulted from activity within the nucleus. The nucleus may be a black hole, which converts an accreted ambient gas to ejected relativistic particles along magnetic fields. Some of the components can be variable in time. The variability can misrepresent the true shape of a spectrum if measurements at all or especially high frequencies are not simultaneous.

In this work we present observational results of more than five hundred sources at six frequencies from 1 to

Send offprint requests to: Y.Y. Kovalev

* Tables 1 and 5 are available at CDS to cdsarc.u-strasbg.fr (130.79.128.5) or via

<http://cdsweb.u-strasbg.fr/Abstract.html>

Correspondence to: yyk@asc.rssi.ru

22 GHz using a single radio telescope. Flux densities at all frequencies are measured practically instantaneously – over a period of a few minutes. This is the shortest time scale of broad band six frequency measurements for the largest sample of sources so far, which has been used for a spectra survey of compact extragalactic radio sources.

These observations are part of a long-term program of instantaneous spectra monitoring of compact extragalactic objects (Kovalev 1998), which have milliarcsecond components and are studied by VLBI networks. They also give a ground spectra support for the VSOP survey and a pre-launch spectra study of the objects for the RadioAstron project. The goal of the long-term program is a mass study of the spectra and their variability for many hundreds of compact extragalactic radio sources. It is also among our intentions to find a relationship between instantaneous multifrequency spectra and the VLBI radio structure.

2. Source sample

We have selected about 700 sources from the Preston et al. (1985) VLBI survey. These sources have a correlated flux density $F_{13}^{\text{corr}} \geq 0.1$ Jy at the wavelength of 13 cm, and are located north of declination -30° . The northern sector of RATAN–600 restricts this declination range from -30° to $+43^\circ$. Measurements of the sources located north of declination $+49^\circ$ were made in 1998 with the southern sector of RATAN–600 and will be published at a later date.

The list of 551 sources for northern sector observations is presented in Table 1. The columns of this table are as follows: (1) the IAU name, (2) possible other name, (3) the optical identification (OI) and (4) the redshift. The OI and redshifts are taken from Veron–Cetty & Veron (1998) or, if not found there, are taken from the NASA/IPAC Extragalactic database (NED). The abbreviations used are “Q” for quasars, “BL” for BL Lacertae objects, “G” for galaxies, “RS” for radio sources. In the latter case we do not have OI. An extended version of this table is available in electronic form at the CDS. This also includes B1950 coordinates taken from Preston et al. (1985) and Moraibito et al. (1986), correlated flux densities at 13 cm with errors from Preston et al. (1985) and optical spectrum classifications from Veron–Cetty & Veron (1998).

3. Observations

We performed continuous six frequency 1–22 GHz spectra observations of compact extragalactic sources from 1st to 22nd December, 1997. We used the 600 meter ring radio telescope RATAN–600 (Korolkov & Parijskij 1979, Parrijskij 1993) at the Russian Academy of Sciences’ Special Astrophysical Observatory, located in Karachaevo-Cherkessia Republic (Russia) near Nizhny Arkhyz and Zelenchukskaya at the North Caucasus. The northern sector

Table 2. Parameters of RATAN–600 broad band receivers in 1997, used in this work

λ , cm	n_h	ν_0 , GHz	$\Delta\nu$, GHz	$T_{\text{LNA}}^{\text{phys}}$, K	T_{LNA} , K	T_{sys} , K	δT_{sys} , mK
1.4	2	21.65	2.5	15	23	77	3.5
2.7	2	11.2	1.4	15	18	70	3
3.9	2	7.70	1.0	15	14	62	3
7.7	1	3.90	0.6	15	8	37	2.5
13	1	2.30	0.4	310	35	95	8
31	1	0.96	0.12	310	21	105	15

Table 3. Measured and estimated beam widths and ratios r for the RATAN–600 northern sector with the secondary mirror No. 1 for different wavelengths λ and elevations h

λ , cm	HPBW _{RA} × HPBW _{Dec}		
	$h = 80^\circ$	$h = 40^\circ$	$h = 20^\circ$
	$r \approx 5$	$r \approx 10$	$r \approx 20$
1.4	8''.0 × 35''	8''.5 × 1'.4	13'' × 4'.3
2.7	16'' × 1'.3	17'' × 2'.8	24'' × 8'.0
3.9	23'' × 2'.0	26'' × 4'.3	39'' × 13'
7.7	48'' × 4'.0	53'' × 8'.8	1'.4 × 27'
13	1'.3 × 6'.5	1'.3 × 13'	1'.8 × 37'
31	3'.2 × 16'	3'.3 × 33'	5'.0 × 100'

of the antenna (a part of the main ring reflector) was used together with the secondary mirror of cabin No. 1. Six broad band receivers are located at this movable cabin. The cabin moves along 150 meter long rails in order to be placed in the focus of the antenna system at different elevations. The main (meridional) transit method of observation was employed. Accuracy and reliability of these spectra measurements were essentially higher than earlier experiments conducted at the RATAN–600 due to the following improvements made to the receivers, antenna control system and the procedure of observations.

We used a new set of broad band receivers at the wavelengths of 1.4, 2.7, 3.9, 7.7, 13 and 31 cm with low noise HEMT amplifiers (LNA), cooled to a temperature of 15 K at the four shortest wavelengths (Berlin et al. 1997, 1993). Parameters of radiometers and antenna beams are given in Tables 2, 3.

Table 2 lists wavelengths λ ; numbers of feedhorns n_h ; exact central frequencies ν_0 ; band widths $\Delta\nu$; physical temperatures of the LNA $T_{\text{LNA}}^{\text{phys}}$; noise temperatures of the LNA T_{LNA} ; total noise temperatures of systems T_{sys} , including the antenna noise at middle elevations; rms noise temperature sensitivities of the system δT_{sys} for a one second integration time. Dual-feedhorn receivers are beam-switched. Single-feedhorn receivers have a noise-added, gain-balanced mode of operation. Linearly polarized systems were available at all frequencies: horizontal at 7.7 cm and vertical at other wavelengths.

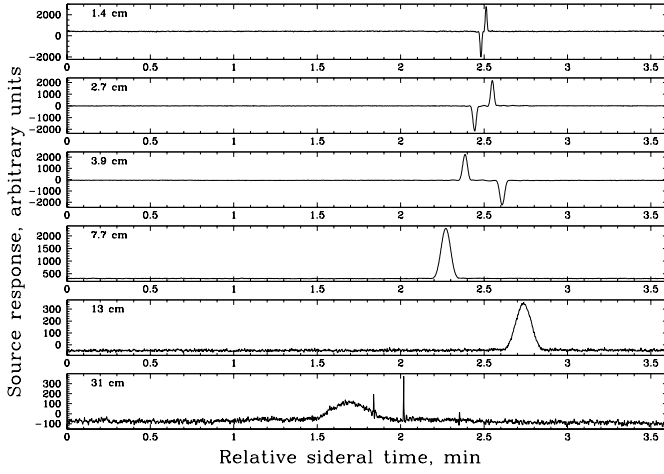


Fig. 1. Example of a full multifrequency scan for 4C 39.25, observed on 16 December 1997 with 0.1 second integration time

Table 3 gives half power beam widths (HPBW) in right ascensions HPBW_{RA} and declinations $\text{HPBW}_{\text{Dec}} = r \text{HPBW}_{\text{RA}}$, for various elevations. The values of HPBW_{RA} were obtained from our measurements. Ignoring the aberration effects, we estimated the factor r using theoretical simulations of the RATAN-600 beam by Esepkinsa et al. (1979) and their experimental testing by Temirova (1983). A map of the knife-like beam of the RATAN-600 northern sector is known to have different shapes of contours cross-sections at high and low power levels. In the absence of aberrations, the shapes can be described as ordinary elliptical contours (elongated on declinations) at half power level and higher levels. The contours are transformed to “the elongated eight” at lower levels or to “a dumb-bell” at 0.1 normalized power level (see Esepkinsa et al. 1979 for details).

The full permanent automatic control of 225 elements of the main ring reflector was achieved using the new control system of the antenna (Zhekanis 1997; Golubchin et al. 1995). Errors in position of each element of the main reflector, if present, were recorded in order to check the quality of the antenna surface for each observation. The positioning of cabin No. 1 with the secondary mirror was measured from one of the eight geodetic reference points, located every 20 meters along the rails. The accuracy of semi-automatic positioning of the cabin directed towards the focus was again checked by us some minutes before each observation. If an error of more than 2 mm with respect to a value given in the schedule was found, it was corrected.

All horns of the radiometers are horizontally located and form a new configuration, which is an optimal one for decreasing transversal aberrations. Observations were carried out in the main meridian (transit mode). As a result, a response to an object is obtained due to its horizontal scanning by the antenna beam because of the daily rota-

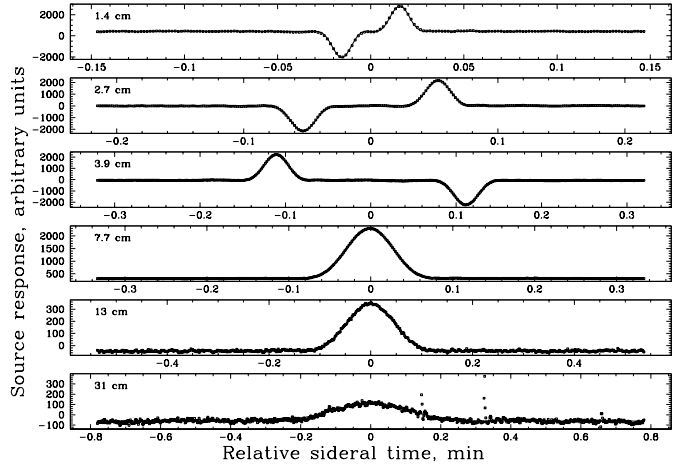


Fig. 2. Example of fitting the simulated beam of RATAN-600 (lines) to the source response (dots) for 4C 39.25 from Fig. 1

tion of the Earth (see an example of 4C 39.25 full scan on Fig. 1; the moment of culmination is at $2^{\text{m}}5$ here). The total duration of each six frequency observations was usually about five minutes, and included also two sets of noise temperature calibration for 30–40 seconds before and after the passing of the source. The data acquisition system (Cherenkov & Tsibulev 1995) controls radiometers and records the output signals. After each observation, the main ring reflector and the cabin No. 1 with receivers and the secondary mirror were repositioned for observation of the next source on a new elevation.

We have optimized the observational schedule, using new software (Zhekanis & Zhekanis 1997). To increase the reliability of results by final averaging of the spectra, we endeavoured to include each source in the schedule two or more times during the set and each flux density calibrator in more than 70% of the days. The typical number of sources observed in a 24 hour observing session was about 80 in the optimized schedule. Several breaks in observations occurred because of weather conditions (snow-falls or unusually low temperatures $t < -15^{\circ}\text{C}$), nine hours of technical maintenance per week, etc. As a result, the total number of successful observations was about 1450 during 21 days, or about 69 observations per day on average and 2.6 spectra per source during the set (formal averaging). In 20% of the sources the spectra have been measured only once.

4. Data reduction and calibration

Data reduction has been done using a YURZUF software package, which had been specially designed for the automatic reduction of the broad band spectra monitoring observations (Kovalev 1998). Fitting a beam which is simulated at the source elevation allows us to compute the amplitude of a source response at each frequency. A Sin-

Table 4. Parameters of calibration sources: flux density, Jy, and correction factors g_{ext} and g_{pol} (from top to bottom)

Source	λ , cm					
	1.4	2.7	3.9	7.7	13	31
0134+32 ($h=79^{\circ}3$)	1.216	2.431	3.540	6.765	10.79	21.90
	1.016	1.004	1.002	1.000	1.000	1.000
	1.032	1.046	1.039	0.959	1.004	1.002
0237–23 ($h=23^{\circ}0$)	0.700	1.470	2.200	4.030	5.590	6.610
	1.000	1.000	1.000	1.000	1.000	1.000
	0.979	0.979	0.979	1.025	0.992	0.983
0518+16 ($h=62^{\circ}8$)	1.135	2.008	2.700	4.413	6.221	10.28
	1.000	1.000	1.000	1.000	1.000	1.000
	0.954	0.956	0.923	1.104	0.930	0.964
0624–05 ($h=40^{\circ}3$)	1.400	2.764	4.156	8.112	12.80	24.10
	1.034	1.009	1.004	1.001	1.000	1.000
	1.027	1.020	1.021	1.025	0.942	1.017
1328+30 ($h=76^{\circ}7$)	2.563	4.244	5.529	8.576	11.50	17.20
	1.016	1.004	1.002	1.000	1.000	1.000
	1.053	0.948	0.957	1.049	0.954	0.954
2037+42 ($h=88^{\circ}5$)	17.40	12.10	5.000
	1.099	1.077	1.013
	1.000	1.000	1.000
2105+42 ($h=88^{\circ}4$)	5.330	5.940	6.100	5.050	2.850	...
	1.297	1.078	1.034	1.008	1.003	...
	0.992	0.992	0.999	1.000	1.000	...

singular Value Decomposition subroutine from Forsythe et al. (1977) was applied. Routine functions, designed by V.R. Amirkhanyan, were also included via an additional interface as a subroutine to the YURZUF software to simulate the main antenna beam together with the secondary lobe. Before the reduction, the quality of such a fitting has been checked and a simulation of the beam has been optimized by tuning control parameters using the sample of 30–50 sources which are strong and compact at all frequencies, and distributed on different elevations (see an example of fitting on Fig. 2).

The following seven flux density calibrators were applied to obtain the calibration curve in the scale of Baars et al. (1977): 0134+32, 0237–23, 0518+16, 0624–05, 1328+30, 2037+42 (for calibration at 7.7, 13 and 31 cm only), 2105+42 (excluding 31 cm calibration). They were recommended by Baars et al. (1977), excluding 0237–23 which is the traditional RATAN–600 flux density calibrator at low elevations. Measurements of some calibrators were corrected, where necessary, on angular size and linear polarization, following the data, summarized in Ott et al. (1994) and Tabara & Inoue (1980) respectively. Response to an extended calibrator was simulated as a two-dimensional convolution of the beam and brightness distribution in the published model of a calibrator. The best fit to the observed response was found by optimization of the angular size of an extended calibrator at each frequency. The correction factor due to an angular extension g_{ext} was

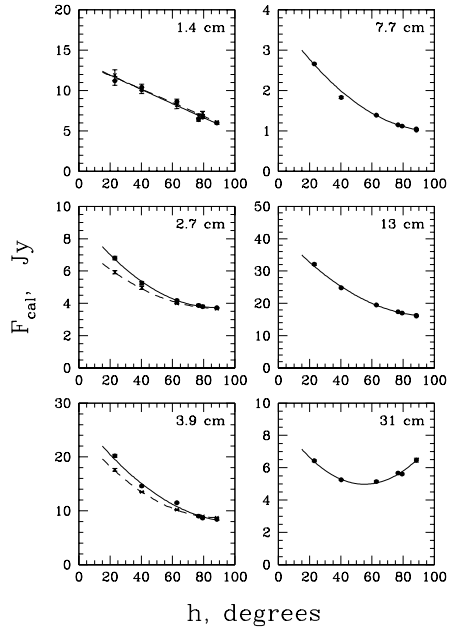


Fig. 3. The flux density calibration factor F_{cal} versus elevation h at all wavelengths. Solid and dashed lines at 1.4, 2.7 and 3.9 cm represent F_{cal} for each horn separately. All data (crosses and points with errors), shown for 6–7 calibrators, were averaged during the observational set. Seven calibrators are shown at 7.7 and 13 cm, but the data for two calibrators at $h=88^{\circ}4$ and $h=88^{\circ}5$ are plotted in the same spot

calculated numerically by integrating over the solid angle of the optimized brightness distribution and the convolution of the distribution with the beam. Following Ott et al. (1994), we applied Gaussian profiles of the brightness distribution over right ascension and declination for 0134+32, 0625–05, 1328+30, 2037+42 and the elliptical disk model for 2105+42, additionally making an axial ratio to be equal to the measured one in Masson (1989). The correction factor due to linear polarization g_{pol} of the calibrators was calculated in the standard way (Kuzmin & Salomonovich 1964, Kraus 1966) as $g_{\text{pol}} = 1/[1 + p \cos(2\varphi)]$, where p is the linear polarization degree and φ is the angle between polarization planes of a source and the antenna. The corrected amplitude of the response to a calibrator is calculated as the observed one, multiplied by the factors g_{ext} and g_{pol} .

The flux densities of the calibrators, in Janskies, the factors g_{ext} and g_{pol} are summarized in Table 4 for each source (at the elevation h) at each wavelength from top to bottom respectively. The flux densities were calculated from polynomial approximations (Taylor 1999) of the VLA measurements (relative to the spectrum of 3C 295) for 0134+32, 0518+16, 1328+30; from spline and polynomial approximations of the data by Ott et al. (1994) for 0624–05, 2037+42, 2105+42 (in relation to the spectra of 3C 295 and 3C 286), and from the polynomial approxi-

mation (Kühr et al. 1979) of the spectrum for 0237–23. For 0134+32 and 1328+30 at 31 cm, we give preference to the flux densities extrapolated from the approximations of Ott et al. (1994). Taking into account all available data, we also used two following extrapolated values: 0.70 Jy for 0237–23 and 1.4 Jy for 0624–05 at the wavelength of 1.4 cm. With these extrapolations, we have obtained reasonable results.

Amplitude measurement of a source in flux density units has been done in relation to an amplitude of a flux density calibrator by comparing both with the amplitude of a stable signal from a noise generator, using standard methods. In our observations the elevations of seven flux density calibrators are fixed. Because of this fact we computed a regression curve to obtain dependence of the flux density calibration factor F_{cal} on the elevation for each horn on each frequency (Fig. 3). F_{cal} is equal to the amplitude of the noise generator signal, calibrated in flux density units. In fact, the obtained calibration curves $F_{\text{cal}}(h)$ show the dependence of the mean measured flux density for a source on the elevation h , if its antenna temperature is equal to that of the noise generator signal T_{ns} (Kovalev 1998): $F_{\text{cal}}(h) = 2kT_{\text{ns}}/A_{\text{eff}}^{\text{aa}}(h)$, where $A_{\text{eff}}^{\text{aa}}(h) = A_{\text{eff}}(h)q^{\text{ab}}(h)q^{\text{atm}}(h)$, $A_{\text{eff}}(h)$ is the effective area of the antenna in the focus, $q^{\text{ab}}(h)$ – the factor of aberration (due to transversal shifts of a feedhorn from the focus), $q^{\text{atm}}(h)$ – the atmosphere attenuation factor, k – the Boltzman's constant. We did not make any additional atmospheric correction during the set (the altitude of RATAN–600 site is 970 m above sea-level).

The total relative rms error of each individual flux density measurement σ/F is estimated from the following relation (Kovalev 1998):

$$\left(\frac{\sigma}{F}\right)_\nu^2 = \left(\frac{\sigma_s}{A_s}\right)_\nu^2 + \left(\frac{\sigma_{\text{ns}}}{A_{\text{ns}}}\right)_\nu^2 + \left(\frac{\sigma_{\text{cal}}}{F_{\text{cal}}}\right)_\nu^2 + (\sigma_{\text{scale}}^r)^2,$$

where the first term inside the brackets on the right hand is the relative error of the amplitude A_s of a source (after fitting the simulated response to the observed one), the second – the relative error of the amplitude A_{ns} of a response to the noise generator signal, the third – the relative error of our flux density calibration F_{cal} , averaged on the set, and the last – the relative error σ_{scale}^r of the absolute flux density scale. Usually, the last term is excluded from presented errors, but we show it in the relation to emphasize its importance, because different calibrators may be used in various works.

The total error σ is calculated, excluding only the σ_{scale}^r error, which is estimated by Baars et al. (1977), Ott et al. (1994) and Taylor (1999) as about 10% at 1.4 cm and 3–5% at other wavelengths. It is better to increase σ_{scale}^r to 10–15% at 1.4 cm for the sources with declinations less than -5° because of the above mentioned extrapolation of the flux density values for 0624–05 and 0237–23. Errors ($\sigma_{\text{cal}}/F_{\text{cal}}$) of the calibration depend on elevation and are formally less than 2.6, 0.7, 1.4, 1.1, 0.7 and 0.9 % at 1.4,

2.7, 3.9, 7.7, 13 and 31 cm respectively (the errors are averaged here over two horns at 1.4–3.9 cm, Fig. 3).

Mean values are always calculated as the mean weighted values, if several measurements have been made, with corrections by the Student's factor to increase the reliability to the standard value 0.683 for one sigma error. The dispersion of frequent measurements of calibrators (and, consequently, σ_{cal} and σ) as well as calculated errors of mean spectra measurements represent also random instrumental instabilities and a variability due to atmosphere conditions during the set.

Systematic errors caused by various reasons including calibration are known to be often the main real errors. We have compared our results with published observations of other authors to check the residual systematic errors, using several tens of strong objects distributed on elevations with constant or slightly variable broad band spectra. The agreement is found to be quite good within the total accuracy of the data.

5. Results

Table 5 with the results of observations is available in the electronic form only at the CDS via anonymous ftp. It includes the flux density data (with one sigma errors without scale errors σ_{scale}^r) at 1.4, 2.7, 3.9, 7.7, 13 and 31 cm for 546 of 551 objects of the source list from Table 1. The results of instantaneous observations of the spectra are shown in Fig. 4. Averaged instantaneous spectra are given in Table 5 and Fig. 4, if two or more observations of a source have been done.

The sources 0156–14, 1635–03 were not observed in December, 1997. We have pointed the antenna to the coordinates of 0611+13 several times, but we have not detected an emission from the source at any frequency (nothing is present at the coordinates of 0611+13 in NED too). The object 3C 274 is resolved by RATAN–600 at all observed frequencies; multifrequency response to 3C 111 has a double maximum. We have excluded the data for these sources from final results.

Absence of data for some sources at some frequencies is a result, in general, of data exclusion for the following reasons: possible confusion in declinations (especially at low elevations) or partial resolution of a source at some frequencies (e.g. 3C 154 at 1.4, 2.7, 3.9, 7.7 cm), a source is too weak to be measured reliably (e.g. III Zw 2 at 31 cm), a strong influence of man-made interferences (frequently at 31 cm, sometimes at 13 cm), strong interferences from a stationary placed satellite at 2.7 and 7.7 cm (in declinations between -10° and 0°). Nevertheless, in some cases the data was not excluded in spite of the increase in errors caused usually by interferences.

We believe that shapes of the instantaneous spectra presented can be explained by continuous activity of the nuclei of the objects in accordance with the basic hypothesis of a source with *two dominating* general components

(compact and extended), following Kovalev et al. (1996), Kovalev & Kovalev (1996). The detailed analysis of the data is deferred to later papers.

Acknowledgements. We would like to thank the RATAN–600 staff for technical support of the observational process. Some of our problems in achieving the twenty four hour observations were resolved through the valuable assistance of Ira Morozova. We are obliged to Harry Teräsranta for providing us with the unpublished data of 22 GHz Metsähovi observations to check our calibration at this frequency, to Greg Taylor for observing the object 0237–23 at our request at the VLA in 1998 and 1999 in order to study known high frequency discrepancy of the source spectrum, and to Vladimir Amirkhanyan for kindly making his routine on simulating the RATAN–600 beam available at our disposal. We thank Tanya Downs and an anonymous referee for carefully reading the manuscript and for valuable comments. YYK and YAK are grateful to the administration and employees of the observatory for their hospitality during the visit for carrying out the observations. This work has been partly supported by the Russian State Program “Astronomy” (grant 1.2.5.1). YYK acknowledges support from International Soros Science Educational Program grants a97–2965, a98–1932 and a99–1882. This research has made use of the NASA/IPAC Extragalactic database (NED), which is operated by the Jet Propulsion Laboratory, Caltech, under contract with the National Aeronautic and Space Administration.

References

- Aller, H.D., Aller, M.F., Latimer, G.E., Hodge, P.E., 1985, ApJS 59, 513
- Amirkhanyan, V.R., Gorshkov, A.G., Konnikova, V.K., 1992, SvA 36, 115
- Baars, J.W.M., Genzel, R., Pauliny-Toth, I.I.K., Witzel, A., 1977, A&A 61, 99
- Berlin, A.B., Lebed, V.I., Maksyashova, A.A., Nizhelsky, N.A., Pilipenko, A.M., Timofeeva, G.M., Shklyarevsky, I.Y., 1993, Astrophyz. Issled. 36, 153
- Berlin, A.B., Maksyashova, A.A., Nizhelsky, N.A., Pilipenko, A.M., Tsibulev, P.G., 1997, in: Problems of the Modern Radioastronomy 3, Publ. of Inst. of Applied Astronomy, St.-Petersburg, p. 115
- Bursov, N.N., 1997, ARep 41, 35
- Chernenkov, V.N., Tsibulev, P.G., 1995, in: XXVIth Radio Astronomical Conference, Publ. of Inst. of Applied Astronomy, St.-Petersburg, p. 389
- Esepkinsa, N.A., Bakhvalov, N.S., Vasiliev, B.A., Vasilieva, L.G., Temirova, A.V., 1979, Astrofiz. Issled. 11, 182
- Forsythe, G.E., Malcolm, M.A., Moler, C.B., 1977, Computer Methods for Mathematical Computations, Prentice-Hall, Inc., Englewood Cliffs, N.J.
- Gear, W.K., Stevens, J.A., Hughes, D.H., Litchfield, S.J., Robson, E.I., Teräsranta, H., Valtaoja, E., Steppe, H., Aller, M.F., Aller, H.D., 1994, MNRAS 267, 167
- Golubchin, G.S., Zhekanis, G.V., Fursa, V.I., 1995, in: XXVIth Radio Astronomical Conference, Publ. of Inst. of Applied Astronomy, St.-Petersburg, p. 402
- Herbig, T., Readhead, A.C.S., 1992, ApJS 81, 83
- Kellermann, K.I., Vermeulen, R.C., Zensus, J.A., Cohen, M.H., 1998, AJ 115, 1295
- Korolkov, D.V., Parijskij, Yu.N., 1979, Sky Telesc. 57, 324
- Kovalev, Yu.A., Berlin, A.B., Nizhelsky, N.A., Kovalev, Y.Y., Babak, S.V., 1996, in: Extragalactic radio sources, eds. Ekers, R.D., Fanti, C., Padrielli, L., Kluwer, Dordrecht, p. 95
- Kovalev, Yu.A., Kovalev, Y.Y., 1996, Odessa Astron. Publ. 9, 163
- Kovalev, Yu.A., 1998, Bull. SAO 44, 50
- Kraus, J.D., 1966, Radio astronomy, McGraw-Hill, New York
- Kuzmin, A.D., Salomonovich, A.E., 1964, Radio Astronomical Methods of Measuring the Antenna Parameters (in russian), Sov. Radio, Moscow
- Kühr, H., Nauber, U., Pauliny-Toth, I.I.K., Witzel, A., 1979, Preprint No. 55, MPIfR
- Kühr, H., Witzel, A., Pauliny-Toth, I.I.K., Nauber, U., 1981, A&AS 45, 367
- Landau, R., Golisch, B., Jones, T.J., Jones, T.W., Pedelty, J., Rudnick, L., Sitko, M.L., Kenney, J., Roellig, T., Salonen, E., Urpo, S., Schmidt, G., Neugebauer, G., Matthews, K., Elias, J.H., Impey, C., Clegg, P., Harris, S., 1986, ApJ 308, 78
- Mingaliev, M.G., Khabrakhmanov, A., 1995, ARep 39, 9
- Masson, C.R., 1989, ApJ 336, 294
- Mitchell, K.J., Dennison, B., Condon, J.J., Altschuler, D.R., Payne, H.E., O’Dell, S.L., Broderick, J.J., 1994, ApJS 93, 441
- Morabito, D.D., Niell, A.E., Preston, R.A., Linfield, R.P., Wehrle, A.E., Faulkner, J., 1986, AJ 91, 1038
- O’Dea, C.P., 1998, PASP 110, 493
- Ott, M., Witzel, A., Quirrenbach, A., Krichbaum, T.P., Standke, K.J., Schalinski, C.J., Hummel, C.A., 1994, A&A 284, 331
- Parijskij, Yu.N., 1993, IEEE Antennas and Propagation Magazine 35, 7
- Preston, R.A., Morabito, D.D., Williams, J.G., Faulkner, J., Jauncey, D.L., Nicolson, G.D., 1985, AJ 90, 1599
- Stevens, J.A., Litchfield, S.J., Robson, E.I., Hughes, D.H., Gear, W.K., Teräsranta, H., Valraoja, E., Tornikoski, M., 1994, ApJ 437, 91
- Tabara, H., Inoue, M., 1980, A&AS 39, 379
- Taylor, G.B., 1999, VLA Calibrator Manual, <http://www.nrao.edu/~gtaylor/calib.html>
- Temirova, A.V., 1983, Astrofiz. Issled. 17, 131
- Valtaoja, E., Haarala, S., Lehto, H., Valtaoja, L., Valtonen, M., Moiseev, I.G., Nesterov, N.S., Salonen, E., Teräsranta, H., Urpo, S., Tiuri, M., 1988, A&A 203, 1
- Veron-Cetty, M.P., Veron, P., 1998, ESO Sci. Rep. 18
- Zhekanis, G.V., 1997, in: Problems of the Modern Radio Astronomy 3, Publ. of Inst. of Applied Astronomy, St.-Petersburg, p. 76
- Zhekanis, G.V., Zhekanis, L.S., 1997, in: Problems of the Modern Radio Astronomy 3, Publ. of Inst. of Applied Astronomy, St.-Petersburg, p. 78

Table 1. Source sample

IAU	Alias	OI	z	IAU	Alias	OI	z	IAU	Alias	OI	z
0003+38		G	0.229	0159–11	3C 57	Q	0.669	0420–01	OA 129	Q	0.915
0003–06	NRAO 5	BL	0.347	0201+11	OD 101	Q	3.56	0421+01	OF 36	Q	2.055
0005–23		Q	1.410	0202+14	NRAO 91	G	0.405	0422+00	OF 38	BL	
0005–26	OB –210	G		0202+31		Q	1.466	0423+23		RS	
0007+10	III Zw 2	G	0.090	0202–17		Q	1.740	0423+05		Q	1.333
0007+17	4C 17.04	Q	1.601	0211+17		Q	0.472	0425+04	OF 42	Q	
0008–26	OB –214	Q	1.093	0216+01		Q	1.623	0428+20	OF 247	G	0.219
0010+40	4C 40.01	Q	0.256	0217–18		Q		0429+41	3C 119	Q	1.023
0011–04		Q		0219+42	3C 66A	BL	0.444	0430+05	3C 120	G	0.033
0012+31	3C 6	G		0219–16		Q	0.698	0434–18		Q	2.702
0013–00		Q	1.574	0221+06	4C 06.11	Q	0.511	0440–00	NRAO 190	Q	0.844
0019+05	OB 34	BL		0223+34	4C 34.07	Q		0446+11		G	1.207
0022+39	OA 26	Q	1.946	0226–03	4C –03.07	Q	2.066	0451–28	OF –285	Q	2.560
0024+34	OB 338	G	0.333	0229+13	4C 13.14	Q	2.065	0454+03	OF 92	Q	1.349
0026+34	OB 343	G	0.6	0234+28	CTD 20	Q	1.207	0454+06	4C 06.21	G	0.405
0027+05		Q		0235+16	OD 160	BL	0.940	0454–23	OF –292	Q	1.003
0035+23	CTD 5	Q	2.27	0237–02		Q	1.116	0456+06	OF 94	Q	1.08
0035+12	4C 12.05	Q	1.395	0237+04	OD 62	Q	0.978	0457+02	OF 97	Q	2.384
0035–02	3C 17	G	0.220	0237–23	OD –263	Q	2.225	0458–02	DA 157	Q	2.286
0038–02		Q	1.176	0238–08	NGC 1052	G	0.005	0458+13		RS	
0047+02	OB 78	BL		0239+10	OD 166	Q		0459+06	OF 99.3	Q	1.106
0048–09	OB –80	BL		0240–21	OD –267	Q	0.314	0459+13		BL	
0048–07	OB –82	Q	1.975	0248+43		Q	1.310	0459+25	3C 133	G	0.277
0054–00		Q	2.795	0250+17		Q		0500+01	OG 3	Q	0.585
0055+30	NGC 315	G	0.016	0256+07	OD 94.7	Q	0.893	0502+04	OG 5	Q	0.954
0055–05		Q		0301+33	4C 33.06	G		0507+17		G	0.416
0056–00	DA 32	Q	0.717	0306+10	OE 110	Q	0.863	0509+15		RS	
0106+01	4C 01.02	Q	2.107	0309+41	NRAO 128	G	0.136	0511–22	OG –220	Q	1.296
0108–07	OC –14	Q	1.776	0312+10	4C 10.10	G		0514–16	OG –123	Q	1.270
0108+38	OC 314	G	0.668	0316+16	CTA 21	Q		0518+16	3C 138	Q	0.759
0109+22		BL		0316+41	3C 84	G	0.017	0521–26	OG –236	RS	
0110+31	NRAO 62	Q	0.603	0317+18	OE 129	G		0528–25	OG –247	Q	2.765
0111+02	UGC 773	G	0.047	0319+12	OE 131	Q	2.67	0528+13	OG 147	Q	2.07
0112–01		Q	1.365	0322+22		RS		0537–15		Q	0.947
0113–11		Q	0.672	0326+27		Q	1.533	0537–28	OG –263	Q	3.104
0116+08	4C 08.06	G	0.594	0327–24	OE –246.3	Q	0.888	0552+39	DA 193	Q	2.365
0118–27	OC –230.4	BL	>0.557	0329–25	OE –248	Q	2.685	0555–13		Q	
0119+11		Q	0.570	0333+32	NRAO 140	Q	1.259	0601+24	4C 24.11	RS	
0119+04	OC 33	Q	0.637	0336–01	CTA 26	Q	0.852	0602+40	OH 404.1	RS	
0119+24		Q	2.025	0338–21	OE –263.9	BL		0605–08	OH –10	Q	0.872
0122–00		Q	1.070	0340+36	OE 367	Q	1.484	0606–22	OH –212	Q	1.926
0123+25	4C 25.05	Q	2.364	0344+19		RS		0607–15	OH –112	Q	0.324
0127+14	4C 14.06	Q		0346–16		Q		0610+26	3C 154	Q	0.580
0130–17		Q	1.020	0348–12	OE –182	Q	1.520	0611+13 ^c			
0133–20	OC –255.3	Q	1.141	0400+25	CTD 26	Q	2.109	0618–25	OH –230	Q	1.90
0134+32	3C 48	Q	0.367	0402+37	4C 37.11	G	0.054	0620+38	OH 335	Q	3.469
0135–24	OC –259	Q	0.831	0403–13	OF –105	Q	0.571	0641+39	OH 368.8	Q	1.266
0136+17		Q	2.716	0405–12	OF –109	Q	0.574	0642+21	3C 166	G	0.245
0138–09	OC –65	BL	>0.501	0406+12		BL	1.02	0650+37		Q	1.982
0142–27	OC –270	Q	1.157	0406–12	OF –111	Q	1.563	0653–03	OH –90	Q	
0144+20		RS		0409+22	3C 108	Q	1.213	0711+35	OI 318	Q	1.620
0146+05	OC 79	Q	2.345	0410+11	3C 109	G	0.306	0722+14	4C 14.23	Q	
0147+18	OC 178	Q		0413–21		Q	0.807	0723–00	OI –39	BL	0.127
0148+27		Q	1.26	0414–18		Q	1.536	0727+40	OI 446	Q	2.501
0149+21		Q	1.32	0415+37 ^b	3C 111	G	0.048	0727–11		RS	
0149+33	OC 383	Q	2.431	0420+02		BL		0729+25		Q	
0156–14 ^a		RS		0420+41	4C 41.11	RS		0733+30		RS	

Table 1. continued

IAU	Alias	OI	z	IAU	Alias	OI	z	IAU	Alias	OI	z
0733–17		RS		0953+25	OK 290	Q	0.712	1148–17	OM –181	Q	1.751
0733+26		RS		0955+32	3C 232	Q	0.530	1156–22		G	0.565
0735+17	OI 158	BL	>0.424	1004–01		Q	1.214	1156–09	OM –94	RS	
0736–06	OI –61	Q	1.901	1004+14	OL 108.1	Q	2.707	1156+29	4C 29.45	Q	0.729
0736+01	OI 61	Q	0.191	1008–01	4C –01.21	Q	0.887	1157–21		Q	0.927
0738+31	OI 363	Q	0.630	1010+35	OL 318	Q	1.414	1200–05	ON –1	Q	0.381
0738+27		RS		1012+23	4C 23.24	Q	0.565	1200+04		RS	
0742+31	4C 31.30	Q	0.462	1013+20	OL 224	Q	3.11	1202–26		Q	0.790
0742+10	OI 471	RS		1015+35	OL 326	Q	1.226	1204+28	ON 208	Q	2.177
0743–00	4C –00.28	Q	0.994	1018+34	OL 331	Q	1.400	1210+13	4C 13.46	Q	1.137
0743+25		RS		1019+42		RS		1211+33	ON 319	Q	1.598
0743+27		RS		1019+30	OL 333	Q	1.319	1213–17	ON –122	G	
0745+24	OI 275	Q	0.409	1020–10	OL –133	Q	0.197	1213+35	4C 35.28	Q	0.857
0748+12	OI 280	Q	0.889	1020+19	OL 133	Q	2.136	1215+30	ON 325	BL	0.237
0748+33	OI 380	Q	1.932	1020+40	4C 40.25	Q	1.254	1216–01		Q	0.415
0752–11	OI –187	RS		1021–00		Q	2.552	1217+02	ON 29	Q	0.240
0754+10	OI 90.4	BL	0.66	1022+19	4C 19.34	Q	0.828	1218+33	3C 270.1	Q	1.519
0759+18		Q		1030+41		Q	1.120	1218–02	4C –02.53	G	0.665
0802+21		RS		1030+39		Q	1.095	1219+28	ON 231	BL	0.102
0805+41		Q	1.420	1032–19		Q	2.198	1219+04	4C 04.42	Q	0.965
0805+26		RS		1034–05	OL –57	G		1222+03	4C 03.23	Q	0.960
0805–07		Q	1.837	1034–29	OL –259	Q	0.312	1222+21	4C 21.35	Q	0.435
0808+01	OJ 14	BL		1036–15	OL –161	G	0.525	1225+36	ON 343	Q	1.975
0812+36	OJ 320	Q	1.025	1038+06	4C 06.41	Q	1.265	1226+02	3C 273	Q	0.158
0812+02	4C 02.23	Q	0.402	1040+12	3C 245	Q	1.028	1228+12 ^b	3C 274	G	0.004
0814+42	OJ 425	BL		1042+07		G	0.698	1228–11	ON –147	Q	3.528
0818–12	OJ –131	BL		1045–18	OL –176	Q	0.595	1236+07		G	0.400
0820+22	4C 22.21	BL	0.951	1046–02	4C –02.43	RS		1237–10	ON –162	Q	0.750
0820+29	OJ 234	Q	2.368	1054+00	OL 91	RS		1240+38		Q	1.316
0821+39	4C 39.23	Q	1.216	1055+20	4C 20.24	Q	1.11	1240–29		Q	1.133
0823+03	OJ 38	BL	0.506	1055+01	OL 93	Q	0.888	1243–07	ON –73	Q	1.286
0827+24	OJ 248	Q	0.941	1058+39		RS		1244–25		Q	0.638
0829+04	OJ 49	BL	0.180	1100+22	OM 201	RS		1252+11	ON 187	Q	0.870
0830+42	OJ 451	Q	0.253	1101+38	Mark 421	BL	0.031	1253–05	3C 279	Q	0.538
0834+25	OJ 259	Q	1.122	1102–24	OM –204	Q	1.666	1255+32	ON 393	RS	
0837+03		Q	1.57	1104+16	4C 16.30	Q	0.632	1256–220	ON –293.9	Q	1.306
0838+13	3C 207	Q	0.684	1106+38		G	2.290	1256–229		Q	1.365
0839+18		Q	1.272	1109+35		RS		1257+14	OW 197	Q	
0851+07		RS		1110–21	OM –218	RS		1302–03		Q	1.250
0851+20	OJ 287	BL	0.306	1111+14	OM 118	Q	0.869	1302–10	OP –106	Q	0.286
0854+21		RS		1116+12	4C 12.39	Q	2.118	1308+32	OP 313	BL	0.997
0855+14	3C 212	Q	1.043	1119+18	OM 133	Q	1.040	1308+14	OP 114	Q	
0859–14	OJ –199	Q	1.339	1120–27	OM –234	RS		1315+34	OP 326	Q	1.050
0900+42	4C 42.28	G		1123+26	CTD 74	Q	2.341	1317–00	4C –00.50	Q	0.892
0906+43	3C 216	Q	0.670	1124–18		Q	1.048	1318–26		Q	2.027
0906+01	DA 263	Q	1.018	1127–14	OM –146	Q	1.187	1330+02	3C 287.1	G	0.215
0912+02		G	0.427	1128+38		Q	1.733	1331+17	OP 151	Q	2.084
0912+29	OK 222	BL		1128–04	OM –48	G	0.266	1334–12	OP –158.3	Q	0.539
0913+39	4C 38.28	Q	1.269	1130+00		Q		1336–23	OP –260.5	Q	
0915–21		Q	0.847	1136–13	CTS 667	Q	0.554	1336–26		Q	1.51
0922+00	OK 37	Q	1.719	1142+05	4C 05.52	Q	1.342	1337–03		Q	
0923+39	4C 39.25	Q	0.698	1142–22	OM –271	Q	1.141	1345+12	4C 12.50	G	0.121
0925–20		Q	0.348	1143–24	OM –272	Q	1.940	1347–21	OP –279	RS	
0931–11	OK –152	RS		1143–28	OM –273	Q	0.45	1348–28		Q	
0938+11		Q	3.191	1144+40		Q	1.089	1349–14	OP –182	RS	
0945+40	4C 40.24	Q	1.252	1145–07	OM –76	Q	1.342	1351–01		Q	3.707
0952+17	OK 186	Q	1.478	1148–00	4C –00.47	Q	1.980	1352–10	OP –187	Q	0.332

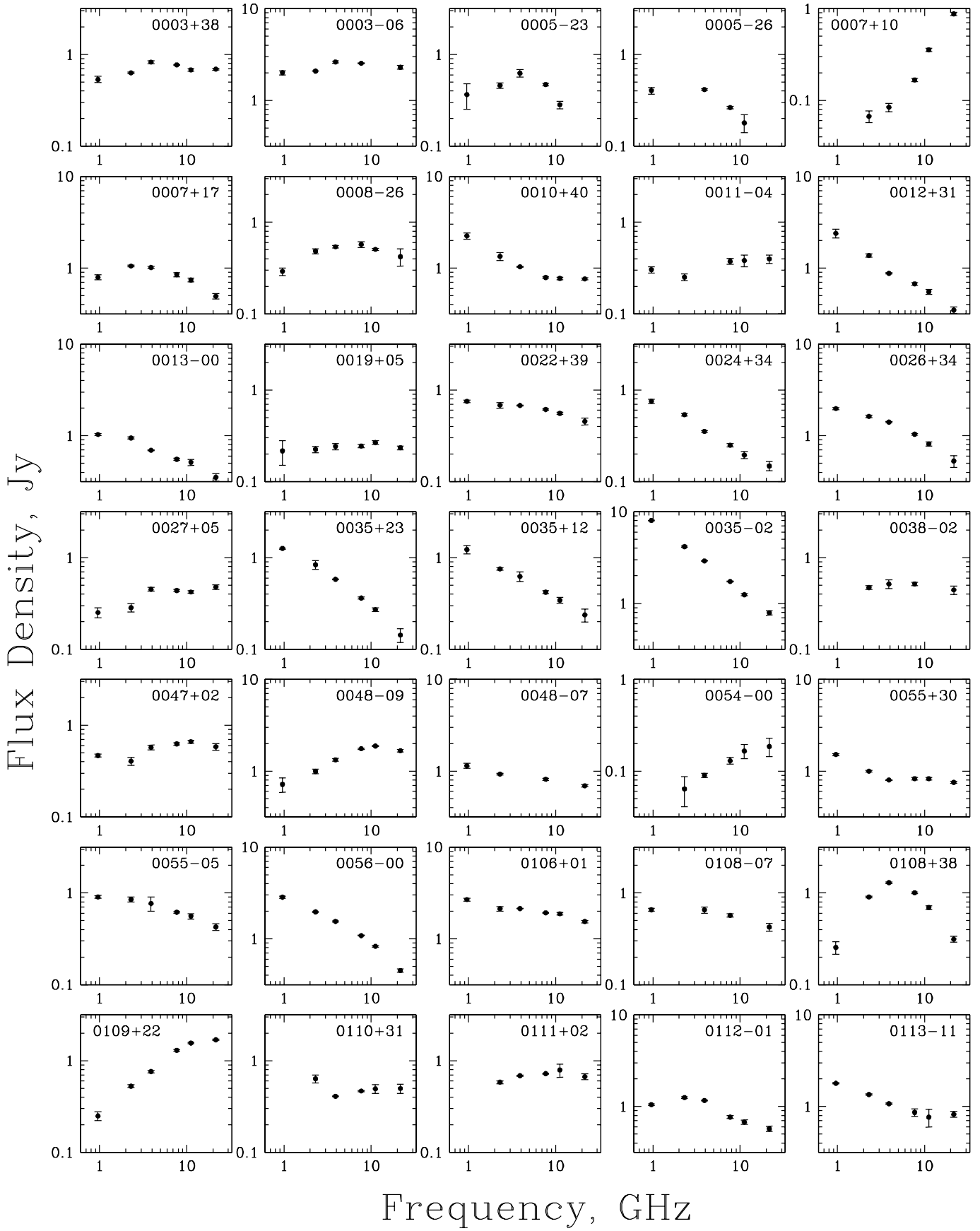
Table 1. continued

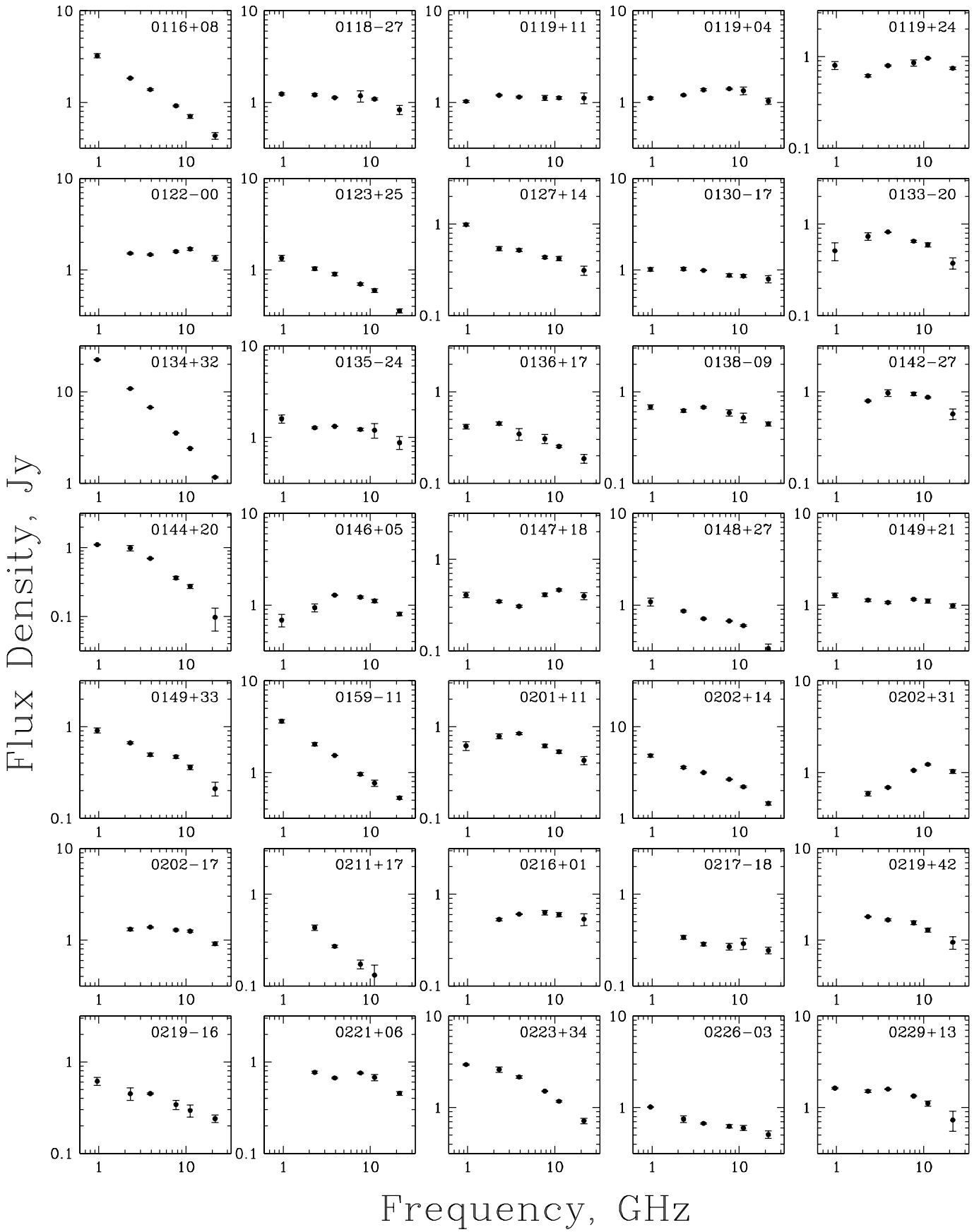
IAU	Alias	OI	z	IAU	Alias	OI	z	IAU	Alias	OI	z
1354–17		Q	3.147	1611+34	DA 406	Q	1.401	2044–16	OW –174	Q	1.932
1354–15	OP –192	Q	1.89	1614+05	OS 23	Q	3.217	2047+09		RS	
1354+19	4C 19.44	Q	0.719	1615+36	4C 36.27	RS		2047+03		BL	
1356+02		Q	1.319	1615+02		Q	1.341	2053–04	4C –04.80	Q	1.176
1402–01		Q	2.522	1616+06	OS 28	Q	2.088	2058–29		Q	1.492
1402+04		Q	3.211	1622–25	OS –237.8	Q	0.786	2059+03	OW 98	Q	1.015
1403–08		Q	1.763	1622–29		Q	0.815	2113+29		Q	1.514
1404+28	OQ 208	G	0.077	1624+41	4C 41.32	Q	2.55	2121+05	OX 36	Q	1.941
1406–07	OQ –10	Q	1.493	1625–14		Q	1.10	2126–15	OX –146	Q	3.266
1406–26		Q	2.43	1633+38	4C 38.41	Q	1.807	2126–18	OX –145	Q	0.680
1413+34	OQ 323	RS		1635–03 ^a		Q	2.856	2127–09		Q	>0.780
1416+06	3C 298	Q	1.439	1638+39	NRAO 512	Q	1.666	2128+04	OX 46	G	0.990
1427+10	OQ 147	Q	1.71	1641+39	3C 345	Q	0.594	2128–12	OX –148	Q	0.501
1430–17	OQ –151	Q	2.331	1647–29		RS		2131–02	4C –02.81	BL	1.285
1430–15	OQ –150.2	Q	1.573	1648+01		RS		2134+00	OX 57	Q	1.932
1434+23	OQ 257	Q		1652+39	Mark 501	BL	0.033	2135–24		Q	0.819
1435–21	OQ –259	Q	1.187	1655+07	OS 92	Q	0.621	2136+14	OX 161	Q	2.427
1437–15	OQ –162	BL		1656+05	OS 94	Q	0.879	2140–04		Q	0.344
1438+38	OQ 363	Q	1.775	1656+34	OS 392	Q	1.936	2143–15	OX –173	Q	0.698
1439+32	OQ 366	Q	2.12	1657–26		RS		2144+09	OX 74	Q	1.113
1441+25		Q	0.062	1705+01		Q	2.576	2145+06	DA 562	Q	0.999
1442+10	OQ 172	Q	3.535	1706+00		G	0.449	2147+14		RS	
1443–16	OQ –171	Q		1706–17	OT –111	RS		2149+06	OX 81	Q	1.364
1445–16	OQ –176	Q	2.417	1717+17	OT 129	BL		2149+05	OX 82	Q	0.740
1449–01	OQ –81	Q	1.314	1721+34	4C 34.47	Q	0.206	2150+17	OX 183	BL	
1452+30	OQ 287	Q	0.580	1722+40		Q	1.049	2155–15	OX –192	Q	0.672
1456+04	4C 04.49	G	0.394	1725+12	OT 143.3	Q		2200–23		Q	2.118
1502+10	4C 10.39	Q	1.833	1725+04		Q	0.293	2200+42	BL Lacertae	BL	0.069
1502+03		G	0.413	1730–13	NRAO 530	Q	0.902	2201+31	4C 31.63	Q	0.298
1504+37	OR 306	G	0.674	1732+09	OT 54	G		2201+17	OY 101	Q	1.076
1504–16	OR –102	Q	0.876	1741–03	OT –68	Q	1.057	2201+04	4C 04.77	G	0.028
1508–05	4C –05.64	Q	1.191	1743+17	OT 172	Q	1.702	2207+35	OY 313	RS	
1510–08	OR –17	Q	0.360	1749+09	OT 81	BL	0.320	2208–13		Q	0.391
1511–10	OR –118	Q	1.513	1751+28		RS		2209+08	DA 574	Q	0.484
1511–21	OR –218	G	1.179	1756+23	OT 295	Q	1.721	2209+23		Q	
1514+00	GNZ 25	G	0.052	1758+38	OT 398	Q	2.092	2214+35	OY 324	Q	0.510
1514+19		BL		1807+27	4C 27.41	Q	1.760	2215+02		Q	3.581
1514–24	AP Librae	BL	0.048	1821+10		Q	1.364	2216–03	4C –03.79	Q	0.901
1518+04	4C 04.51	G	1.294	1830+28	CTD 108	Q	0.594	2223–05	3C 446	Q	1.404
1519–27		BL		1848+28		Q	2.56	2223+21	DA 580	Q	1.953
1525+31	OR 342	Q	1.380	1901+31	3C 395	Q	0.635	2227–08		Q	1.562
1532+01		Q	1.420	1908–20	OV –213	Q		2229–17	OY –150	Q	1.780
1535+00		Q	3.497	1908–21	OV –214	RS		2230+11	CTA 102	Q	1.037
1538+14	4C 14.60	BL	0.605	1920–21	OV –235	RS		2233–14	OY –156	BL	>0.609
1543+00		G	0.550	1921–29	OV –236	BL	0.352	2234+28	CTD 135	Q	0.795
1546+02	OR 78	Q	0.412	1923+21	OV 239.7	RS		2236+12	OY 160	Q	
1548+05	4C 05.64	Q	1.422	1936–15	OV –161	Q	1.657	2239+09		Q	1.707
1548+11	OR 181	Q	0.436	1937–10		Q	3.787	2240–26	OY –268	BL	0.774
1550–26		Q	2.145	1947+07	OV 80	Q		2243–12	OY –172.6	Q	0.630
1551+13	OR 186	Q	1.29	1958–17	OV –198	Q	0.652	2245–12		Q	1.892
1555+00		Q	1.772	2002–18	OW –105	Q	0.868	2245+02		Q	
1555–14		G	0.097	2008–15	OW –115	Q	1.180	2246+20		RS	
1556–24		Q	2.818	2008–06	OW –15	G	1.047	2247+13	4C 13.84	Q	0.767
1600+33	OS 300	G		2012–01		BL		2251+15	3C 454.3	Q	0.859
1604+31		G		2029+12	OW 149	BL	1.215	2251+24	DA 587	Q	2.327
1606+10	DA 401	Q	1.226	2032+10	OW 154.9	BL	0.601	2251+13	4C 13.85	Q	0.677
1607+26	OS 211	G	0.473	2037–25		Q	1.574	2252–09		Q	0.606

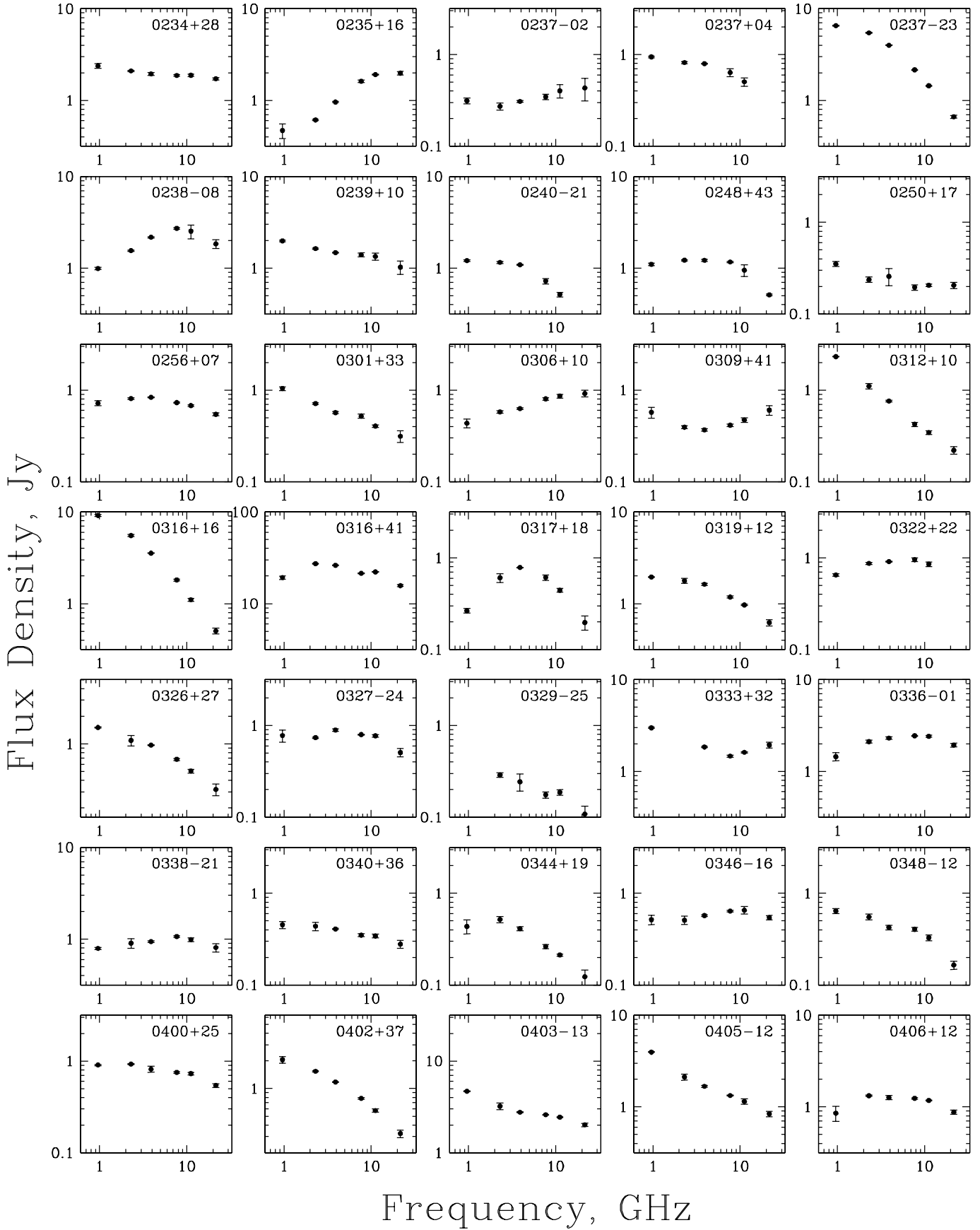
Table 1. continued

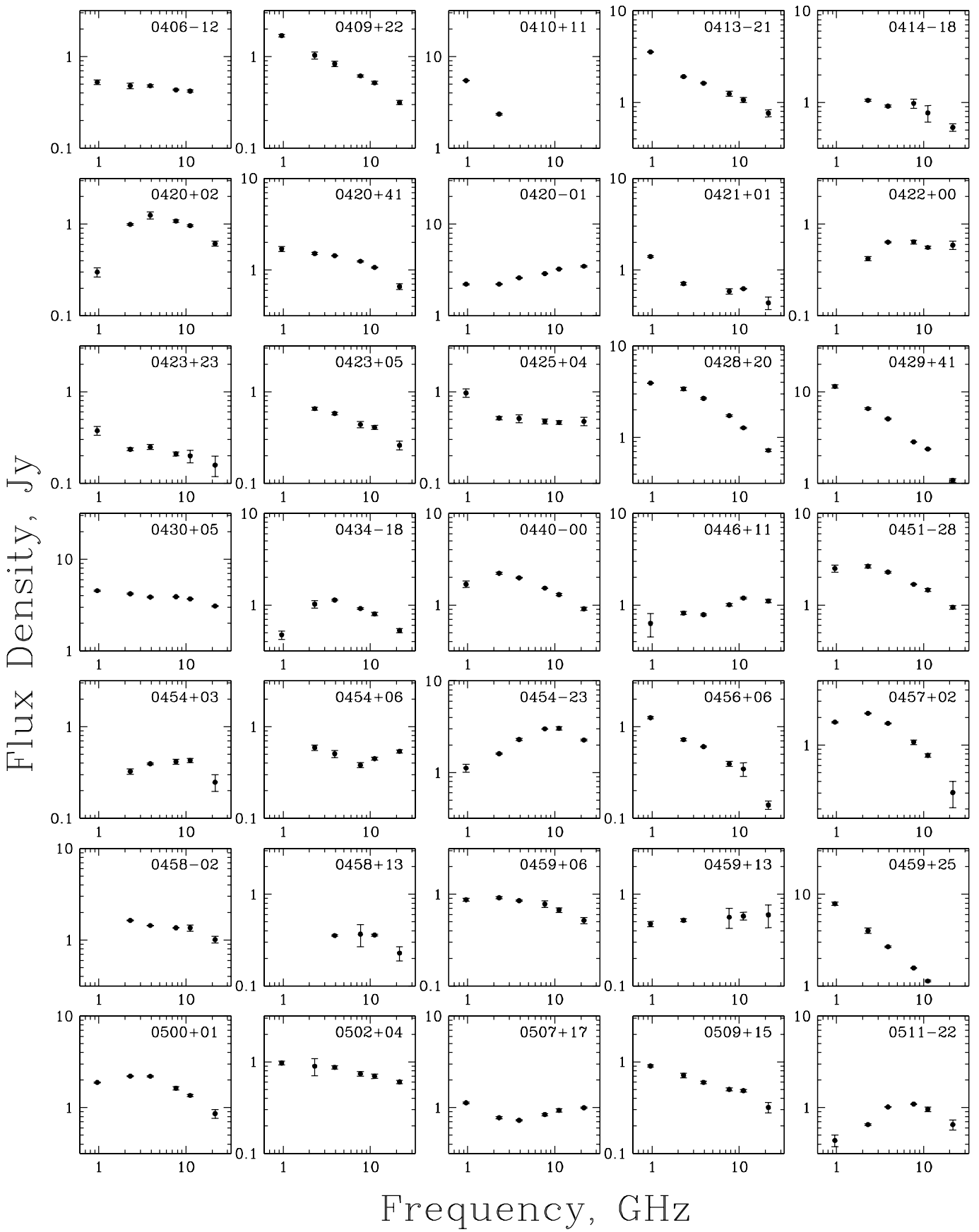
IAU	Alias	OI	<i>z</i>
2253+41	OY 489	Q	1.476
2254+02	OY 91.3	Q	2.089
2254+07	OY 091	BL	0.190
2255+41	4C 41.45	Q	2.15
2255–28		Q	0.926
2256+01		Q	2.663
2300–18	OZ –102	G	0.129
2303–05	4C –05.95	Q	1.139
2307+10	4C 10.70	RS	
2318+04	OZ 031	Q	0.623
2318–19	OZ –130	G	
2319+31		G	
2319+27	CTD 139	Q	1.253
2320+07	DA 599	Q	2.090
2320–02		Q	
2320–03		Q	1.411
2325–15		Q	2.465
2327+33		Q	1.809
2328+10	4C 10.73	Q	1.489
2328+31	OZ 347	RS	
2329–16	OZ –149	Q	1.153
2330+08	OZ 50.8	RS	
2331–24	OZ –252	G	0.048
2332–01		Q	1.184
2335–18	OZ –160	Q	1.450
2335–02		Q	1.072
2337+26		Q	
2338+33		RS	
2344+09	4C 09.74	Q	0.673
2344+092		RS	
2345–16	OZ –176	Q	0.576
2349–01	4C –01.61	Q	0.174
2351–00		Q	0.463
2351–15	OZ –187	Q	2.675
2354–11		Q	0.960
2355–10		Q	1.622
2356+19	OZ 193	Q	1.066
2356+38	OZ 395	Q	2.704

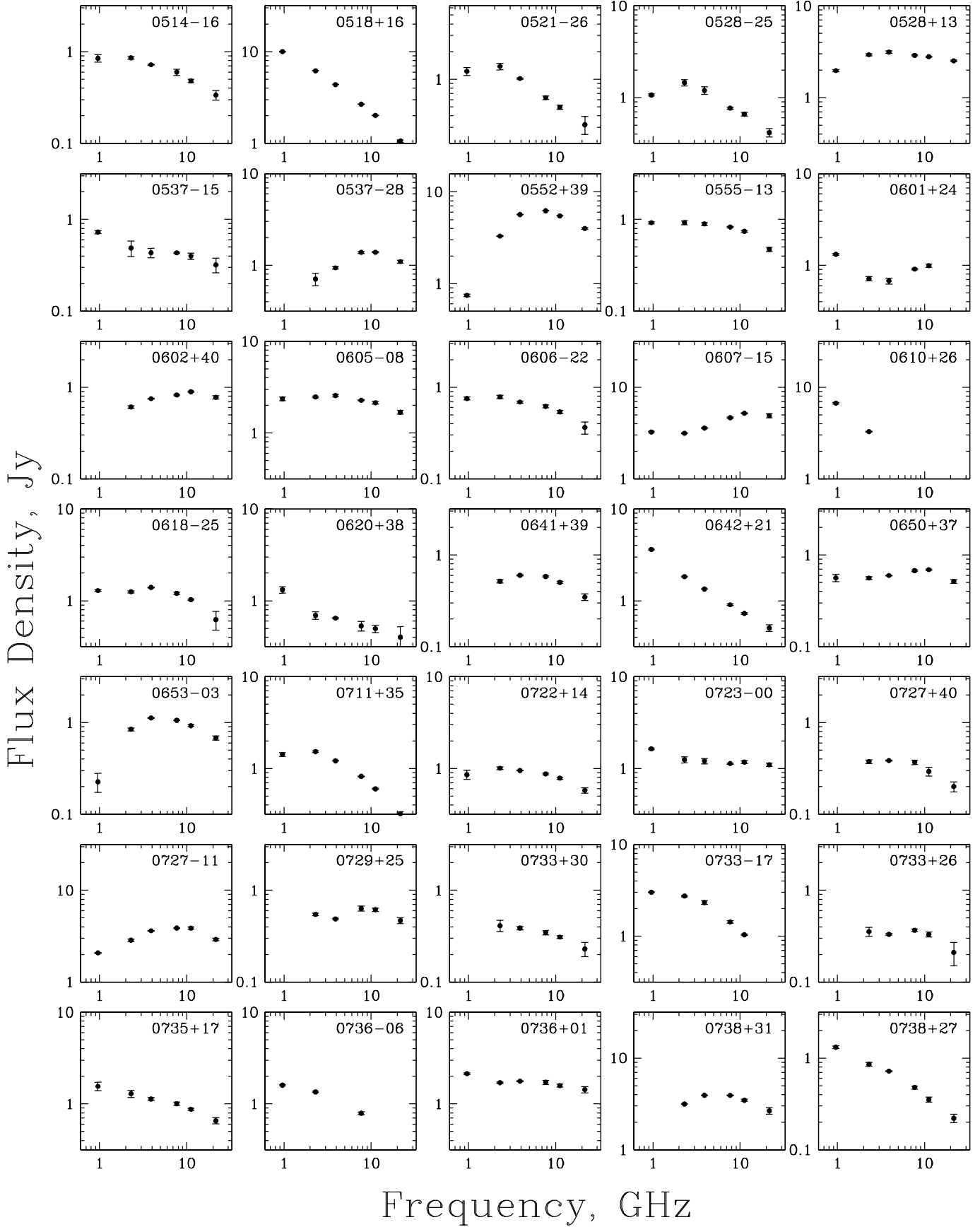
^a The source was not observed in December, 1997^b The source was partly resolved at all frequencies^c We have not registered emission from this object at any frequency (nothing is present at these coordinates in NED too)

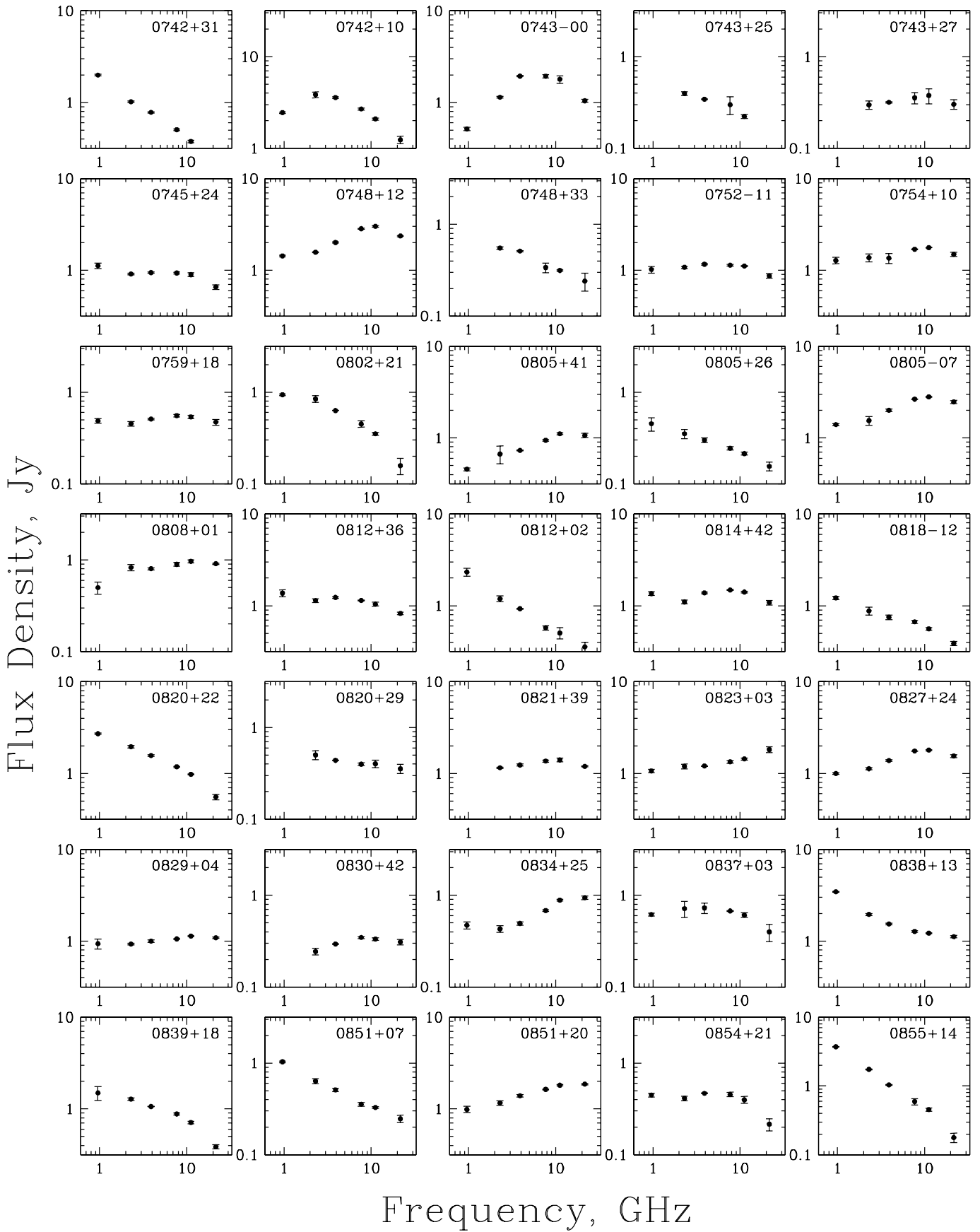
**Fig. 4.** Instantaneous spectra

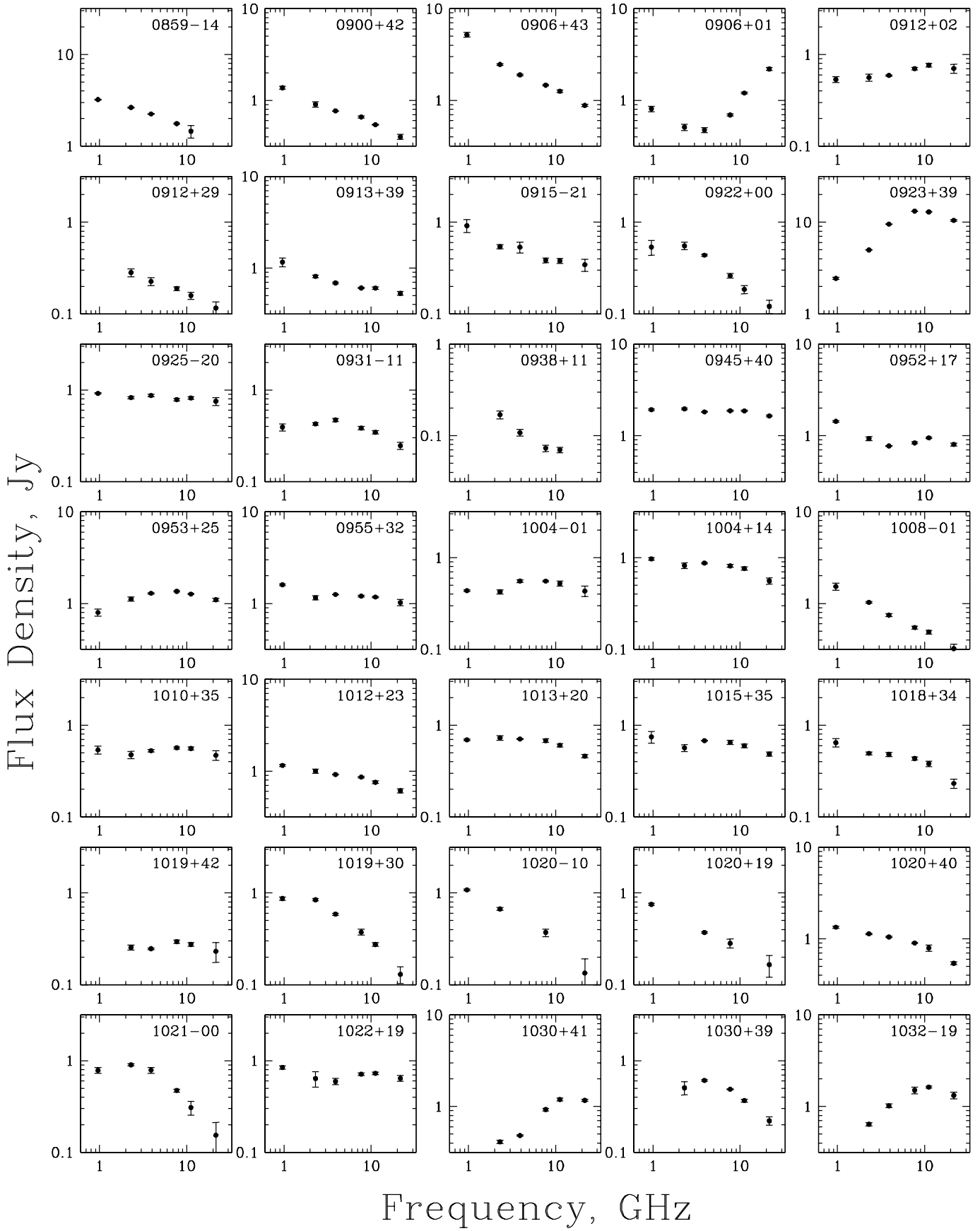
**Fig. 4.** continued

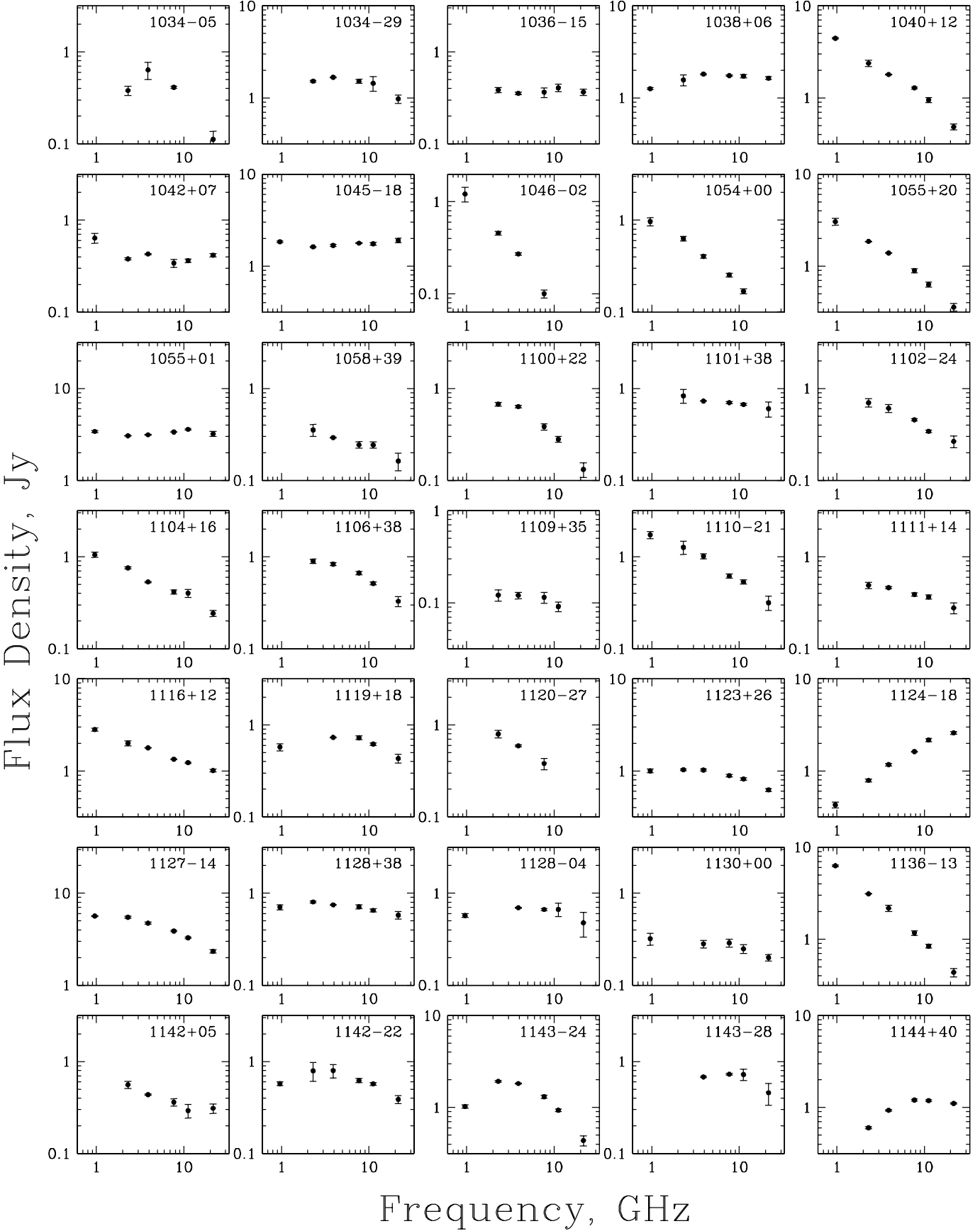
**Fig. 4.** continued

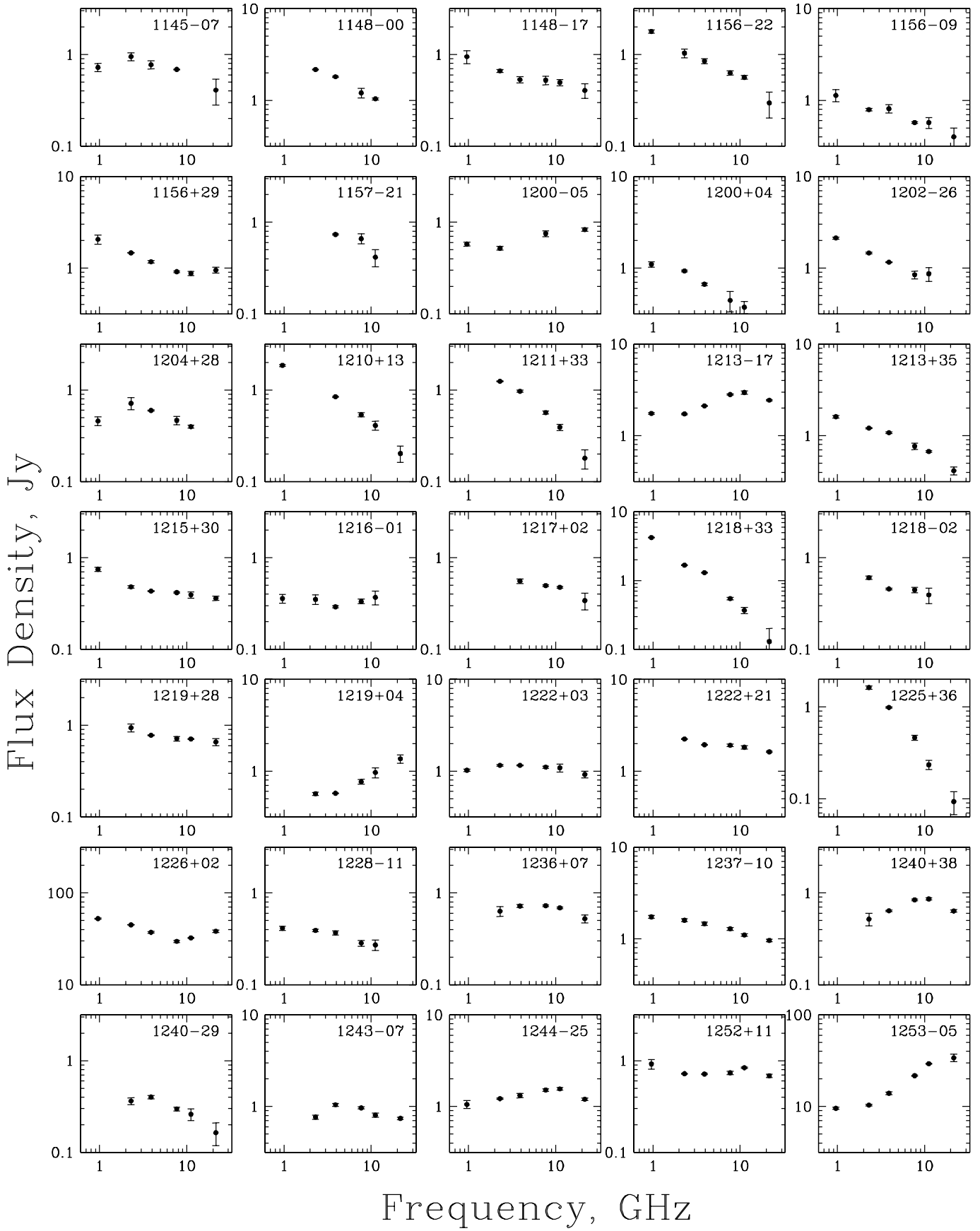
**Fig. 4.** continued

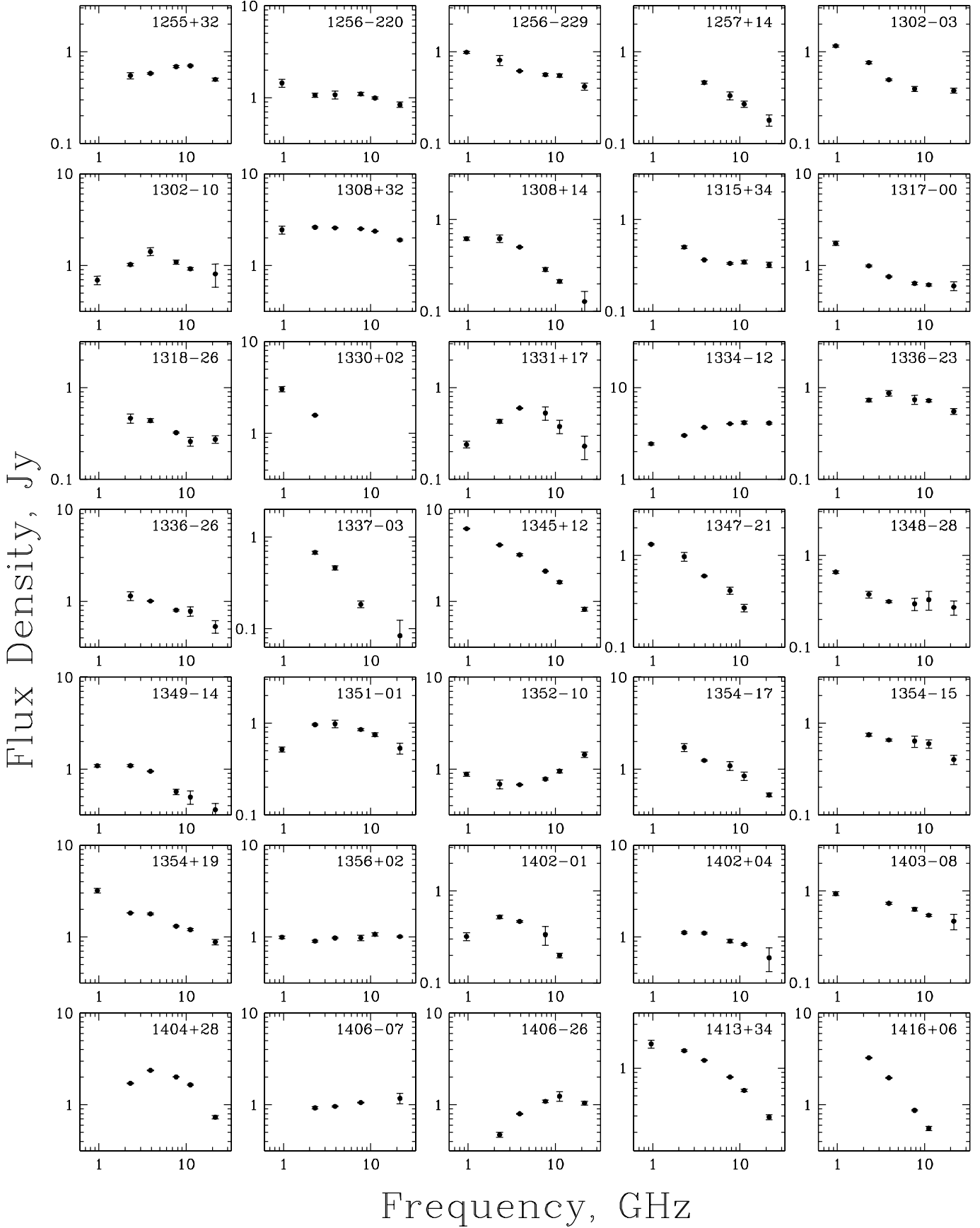
**Fig. 4.** continued

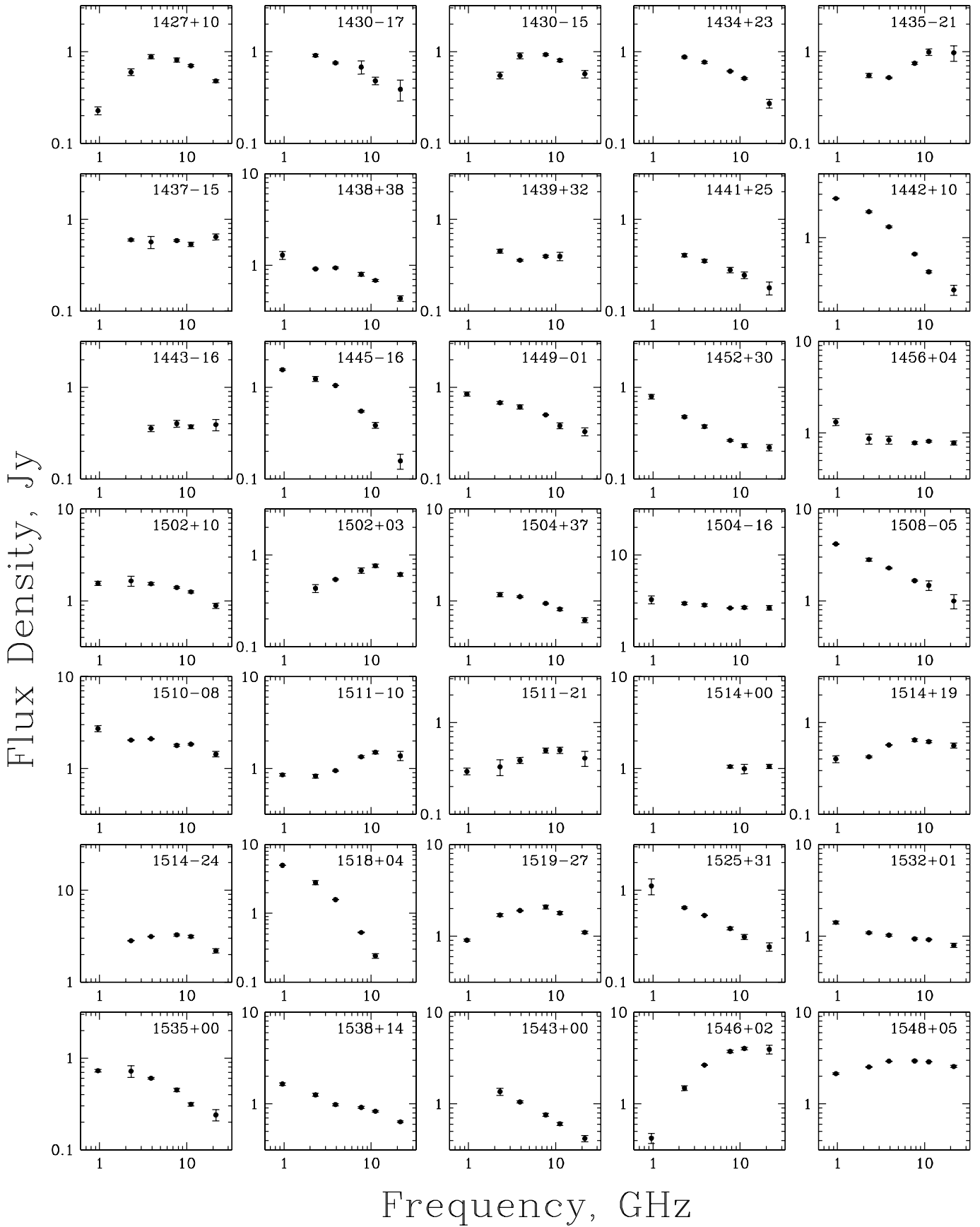
**Fig. 4.** continued

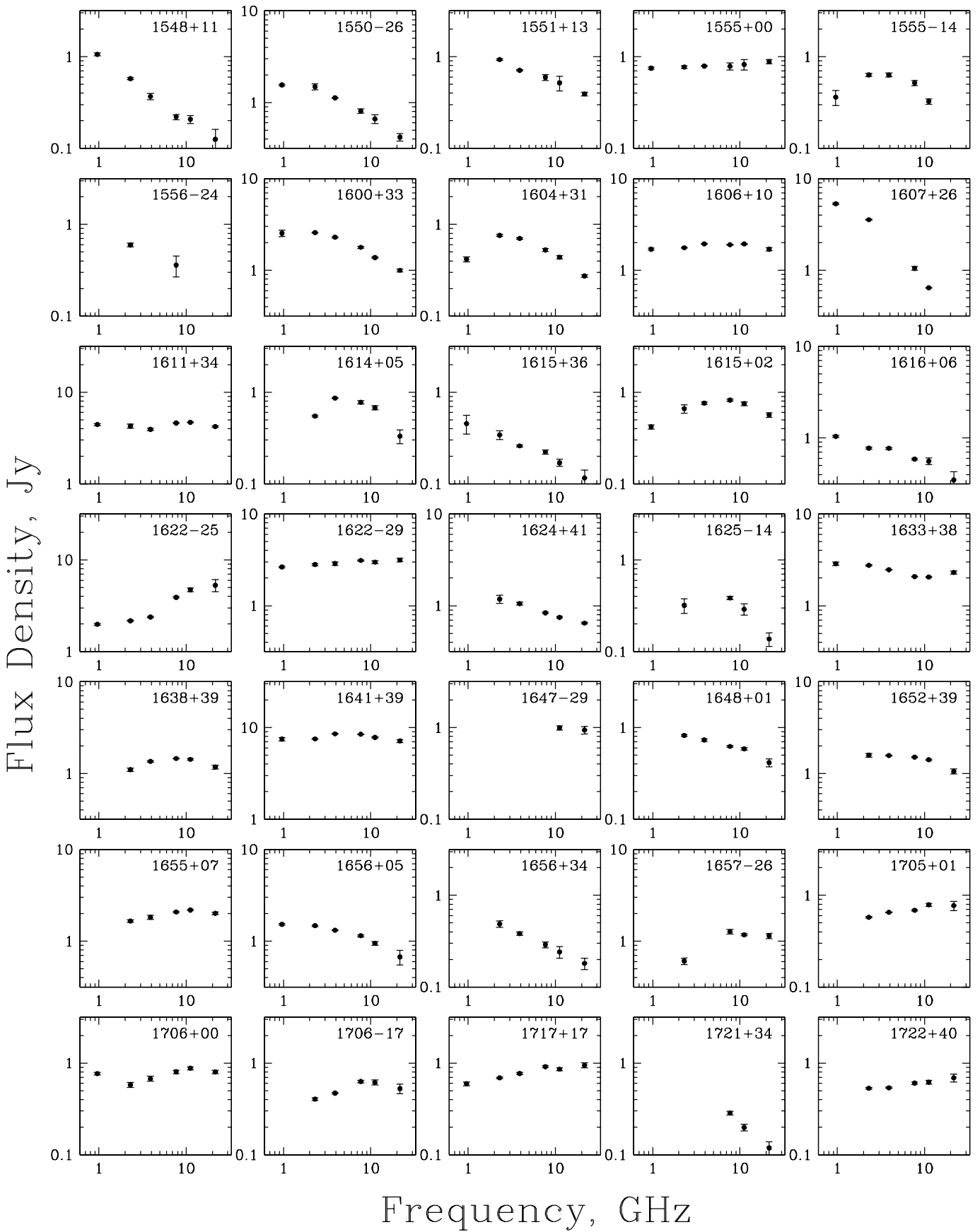
**Fig. 4.** continued

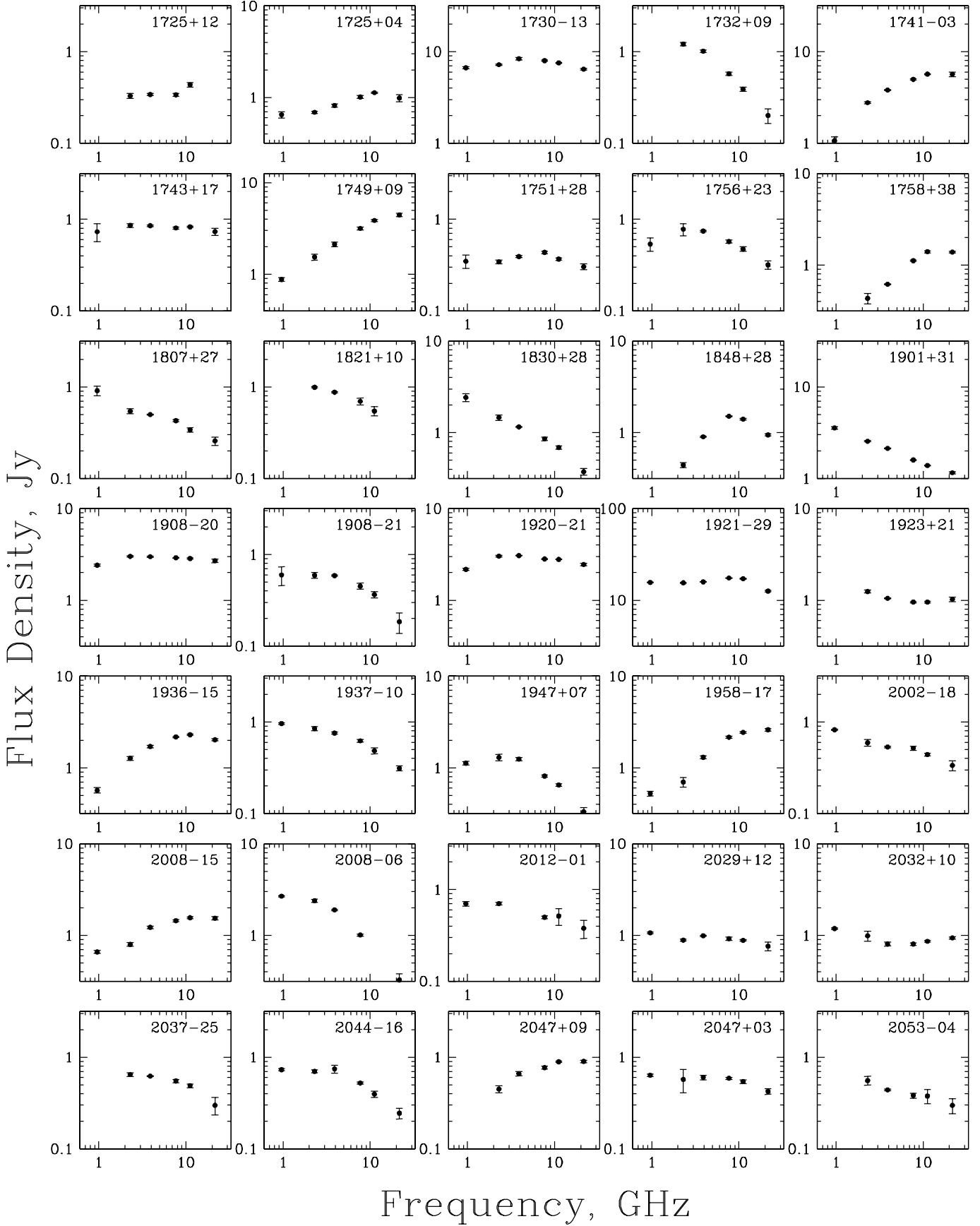
**Fig. 4.** continued

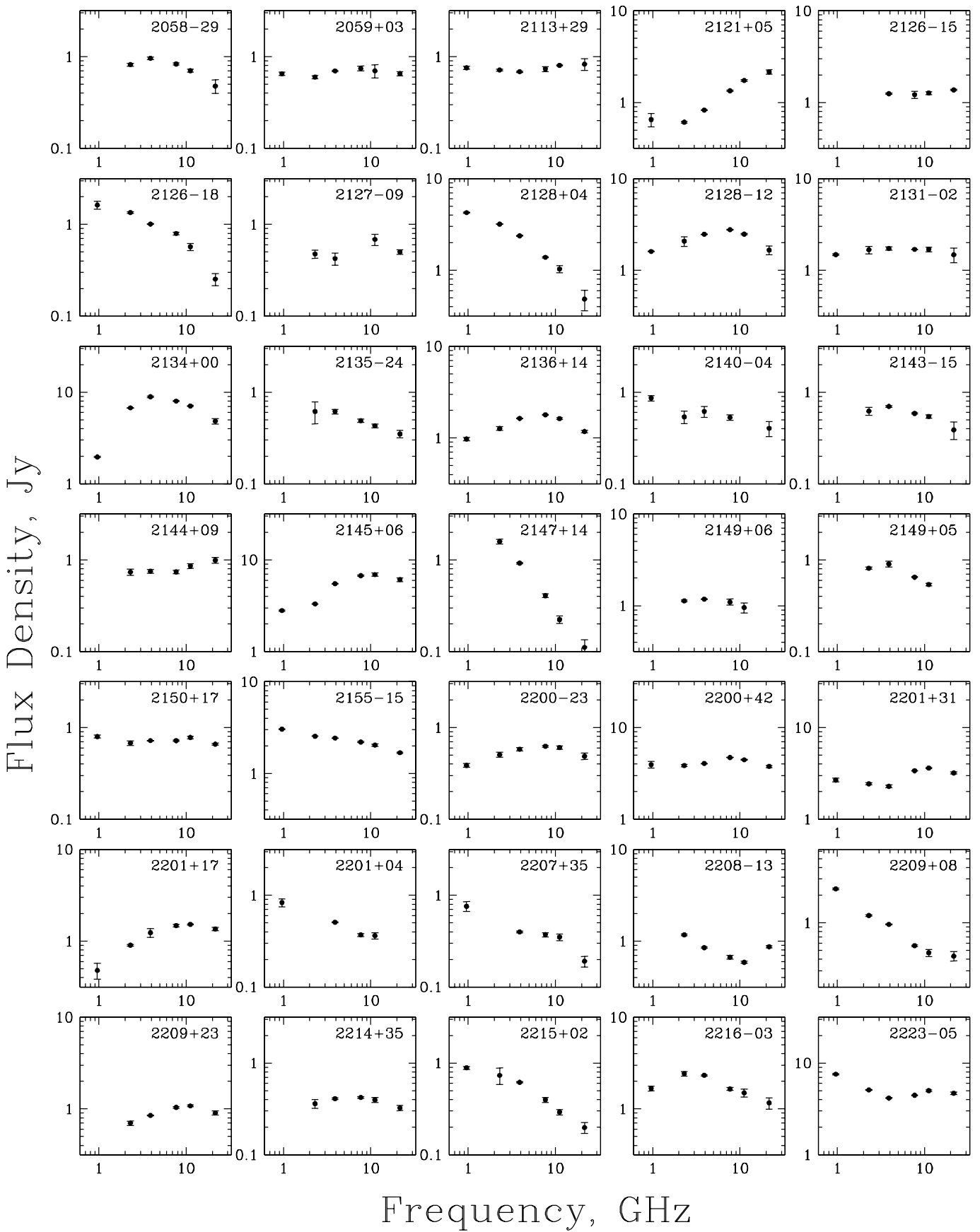
**Fig. 4.** continued

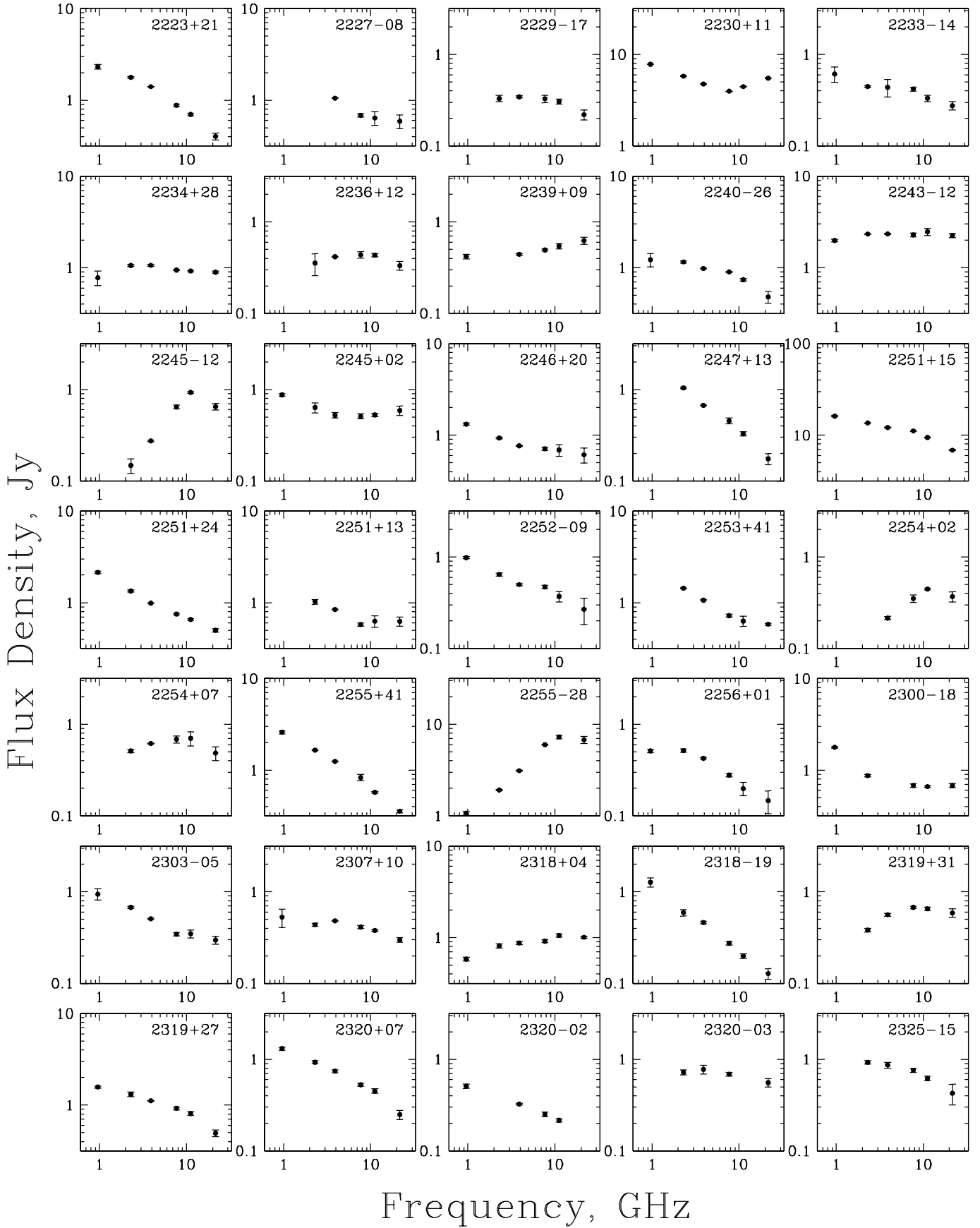
**Fig. 4.** continued

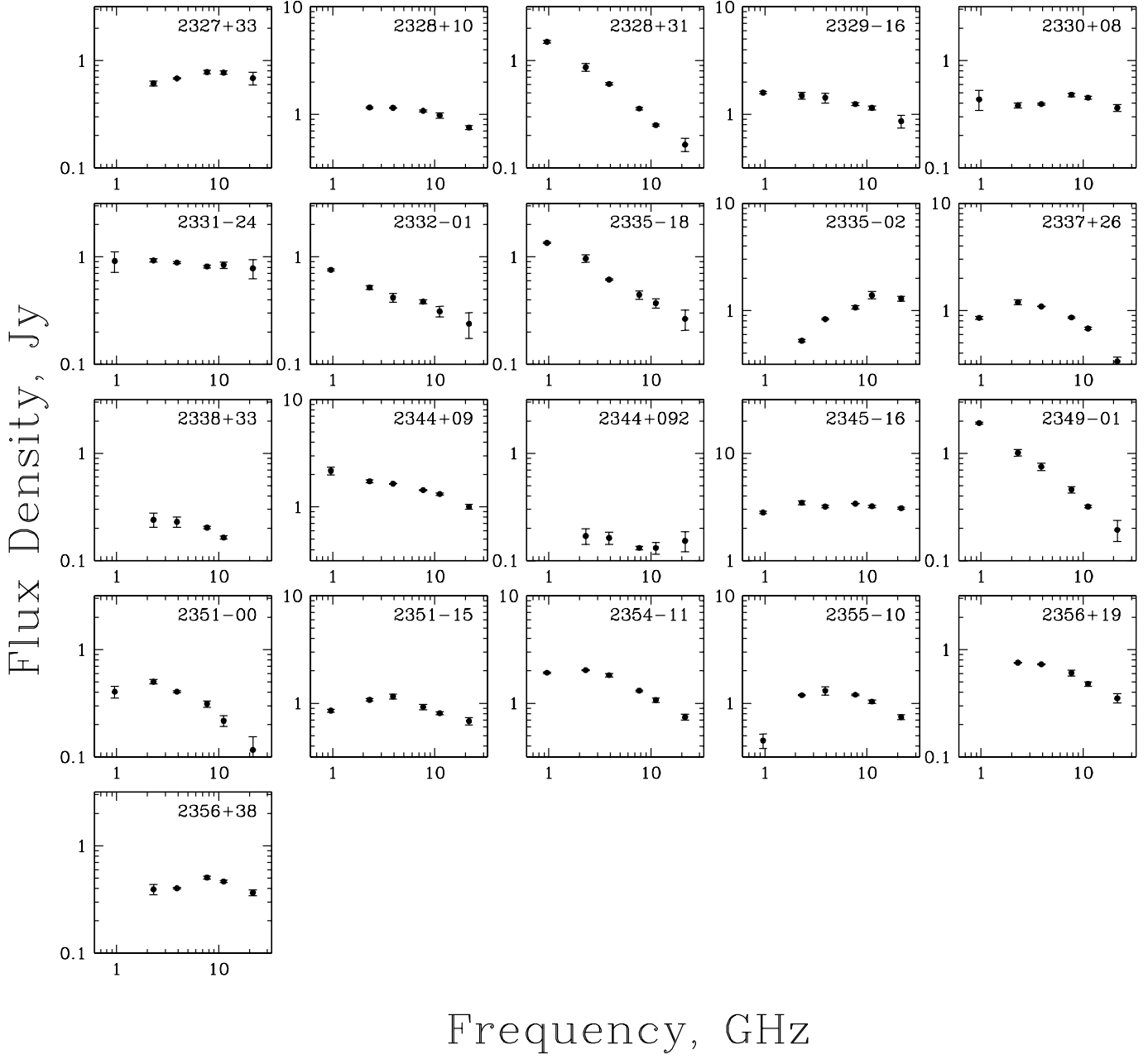
**Fig. 4.** continued

**Fig. 4.** continued

**Fig. 4.** continued

**Fig. 4.** continued

**Fig. 4.** continued

**Fig. 4.** continued